287

London Road, Bracknell
Berkshire RG12 2SZ

LONDON, METEOROLOGICAL OFFICE.
Met.O.11 Technical Note No. 245

Penetrative convection in an extended Lagrangian semi-geostrophic theory.

06880287

PH

MET O 11 TECHNICAL NOTE NO. 245

# Penetrative Convection in an extended Lagrangian semi-geostrophic theory

by G. J. Shutts

December 1986

Abstract

Analytic solutions representing rectilinear flow in geostrophic and hydrostatic balance are constructed using the conformal mapping technique of Gill (1981). Two types of mapping are used to characterise the state of a fluid after a parcel convects to a position of neutral buoyancy. The first mapping corresponds to the homogeneous intrusion in a rotating, stratified fluid studied by Gill. The second mapping describes an internal discontinuity of a finite length embedded in a fluid of uniform potential vorticity. In the idealised physical problem represented by these conformal transformations, an elliptical region of undisturbed fluid is considered to be 'saturated' and in a state of unstable equilibrium. On perturbing the system, the saturated parcel convects to a new level distant from its initial position and is rendered homogeneous in absolute momentum and potential temperature by internal mixing. The resulting equilibrium configuration involves a two-dimensional fluid lens which locally distorts the environmental stratification. An internal front is shown to represent the equilibrium flow structure in the region initially occupied by the saturated parcel.

The model predicts mesoscale regions of descent below the lens. The fluid within the lens has zero absolute vorticity whereas strong cyclonic vorticity exists near and at the internal front. Solutions are obtained for undisturbed states of uniform potential vorticity either at rest or uniformly sheared with constant horizontal temperature gradient. It is inferred that moist boundary layer air ahead of some cold fronts may slantwise convect in narrow plumes just above the frontal surface and in

the process greatly accelerate the formation of a lower tropospheric frontal discontinuity line compared to geostrophic forcing such as deformation. The model may also be relevant to the dynamical forcing of mesoscale downdraughts associated with deep cumulonimbus convection.



## 1. Introduction

Balanced equations of motion such as the semi-geostrophic system (Hoskins, 1975) and the angular momentum coordinate equations (Shutts and Thorpe, 1978) are conventionally used to describe flows which are inertially and convectively stable at all times. Under these conditions the ageostrophic circulation generated by dynamical or irreversible physical forcing functions is determined by an elliptic equation subject to the positivity of a pseudo-potential vorticity (e.g. Hoskins and Draghici, 1977; Shutts and Cullen, 1987). Ageostrophic motion provides the continuous adjustment of the mass field required to keep the fluid in geostrophic and hydrostatic balance. In adiabatic and inviscid semi-geostrophic flow the pseudo-potential vorticity is conserved following the motion and an initially stable fluid will remain so, (Bennetts and Hoskins, 1979). The presence of heat sources and sinks may however reduce the potential vorticity to zero rendering the equation for the ageostrophic motion parabolic, and the problem ill-posed (Thorpe and Emanuel, 1985). The breakdown in the balanced flow method associated with the onset of convection demonstrates the problem and how it may be circumvented with the introduction of some extra physical assumptions.

Consider as in Fig. 1(a) a vertical fluid column comprising five elements each of uniform potential temperature $\theta_i$. The fluid column will be stable provided that the elements are ordered so that:

$$\theta_{i+1} > \theta_i \qquad i = 1, 4.$$

If the fluid is incompressible, the elements may be heated or cooled without causing any motion provided that this ordering is maintained. Suppose now that an impulse of heat energy is offered to element 1 so that:

$$\theta_4 < \theta_1 < \theta_5.$$

The fluid would now be in a state of unstable equilibrium corresponding to negative potential vorticity in the rotating continuous problem. In practice, the system would create convection which would transfer fluid in element 1 to between element 4 and 5 and cause a certain amount of mixing between elements. A new balanced hydrostatic state would ultimately be set up after transient motion is damped out by viscous effects.

Instead of abandoning any hope of solving the physical problem when the static stability, proportional to $(\theta_{i+1} - \theta_i)$, approaches zero we could extend our class of solutions (trivial as they are in this example) by assuming that the fluid undergoes an instantaneous rearrangement to the state depicted in Fig. 1(b). Although the introduction of a heat impulse is unphysical, a similar effect would be realised if element 1 were saturated and contained enough moisture to allow it to convect up to the same level. The rearranged state could only be achieved if no mixing occurs. This will never be the case in the real world though under some situations it may be a useful idealization. For instance, tropical boundary layer air may ascend in hot convective towers (Riehl and Malkus, 1958) without significant mixing with the environment.



A non-trivial extension of this heat impulse thought-experiment is provided by its two-dimensional generalisation. Consider a parcel representation of an atmosphere at rest such that each parcel is rectangular in cross-section and has a uniform absolute momentum, M $(= v_g + fx$, eg Gill (1981)) and potential temperature, $\theta$. In the 100 element representation depicted in Fig. 2(a), rows of elements have the same potential temperature and columns have the same absolute momentum. Interfaces between neighbouring elements satisfy a Boussinesq form of the Margules equation for the slope of a frontal boundary:

$$\frac{dz}{dx} = \frac{f[M]}{g[\theta/\theta_o]}$$

where the square brackets denote element differences, f is the Coriolis parameter, g is the acceleration due to gravity and $\theta_o$ is some constant reference potential temperature. In this case dz/dx equals zero or infinity corresponding to horizontal or vertical edges respectively. If an impulse of heat is introduced into element 30, sufficient for its potential temperature to be raised to a value between that of element 50 and 70, then a new equilibrium may be sought for which element 30 lies between the isentropic layers containing elements 50 and 70. During this convective transfer it will be assumed, consistent with two-dimensionality (into the picture) and the non-mixing hypothesis, that the absolute momenta and areas of all elements are preserved. Also the potential temperature is conserved for all elements except element 30. Using the 'geometric' algorithm described in Cullen et al (1987), a final equilibrium state may be calculated, (Fig. 2(b)). Element 30 now appears as a lens of fluid squeezed between two isentropic layers and elements 29 and 31, which were

originally separated, are brought together. Note that all fluid interfaces satisfy Margules relation in this final state. Elements in the two isentropic layers above and below the lens are forced away from the centre of mass of element 30. Since M is conserved before and after the convective jump, anticyclonic vorticity is created above and below the lens. On the contrary, elements in the 'donor' layer move towards the original position of element 30 conserving M and therefore create cyclonic vorticity.

The lens is reminiscent of the analytic structure of a homogeneous intrusion embedded in a uniform potential vorticity fluid found by Gill (1981). In this paper, analytic solutions are provided which model the lens, and the flow in the region from which the fluid convected. Solutions are obtained for a variety of different initial states and represent the complete 'before and after' equilibrium states associated with convection, provided that the lens is sufficiently far removed from the donor region.

## 2. Two-dimensional upright convection

### (a) Gill's lens solution

It is convenient to express the conditions for geostrophic and hydrostatic balance in the form used by Hoskins and Bretherton (1972) so that:

$$fv_g = \frac{\partial \phi}{\partial x} \qquad (1)$$

and

$$\frac{g\theta}{\theta_o} = \frac{\partial \phi}{\partial z} \qquad (2)$$



where $\phi$ is the geopotential and z is a pseudo-height coordinate depending on pressure alone. In this analysis it is expedient to make what Hoskins and Bretherton refer to as the Boussinesq approximation by setting their pseudo-density r(z) equal to unity. Air parcels are then volume preserving in (x,y,z) space. The thermal wind equation derived from eqs. (1) and (2) is then:

$$f\frac{\partial v_g}{\partial z} = \frac{g}{\theta_o}\frac{\partial \theta}{\partial x} \qquad (3)$$

The Ertel potential vorticity (q) for rectilinear flow governed by eqs. (1) and (2) is given by:

$$q = \left(f + \frac{\partial v_g}{\partial x}\right)\frac{\partial \theta}{\partial z} - \frac{\partial v_g}{\partial z}\frac{\partial \theta}{\partial x}$$

$$= J\left(\frac{M}{x}, \frac{\theta}{z}\right) \qquad (4)$$

where J denotes the Jacobian of transformation between the space of $(M,\theta)$ and $(x,z)$.

Eqs. (1)-(3) are now non-dimensionalised using H as a height scale, NH/f as a horizontal length scale, NH as a velocity scale, $N^2H\theta_o/g$ as a potential temperature scale ands $N^2H^2$ as a geopotential scale to give:

$$v = \frac{\partial \phi}{\partial x} \qquad (5)$$

$$\theta = \frac{\partial \phi}{\partial z} \qquad (6)$$

$$\frac{\partial v}{\partial z} = \frac{\partial \theta}{\partial x} \qquad (7)$$

where the subscript g will be omitted since all velocities considered in this paper will be geostrophic. Furthermore if M and q are non-dimensionalised by NH and $fN^2\theta_o/g$ respectively, then eqs (4) and (7) may be written as:

$$J\left(\frac{M,\theta}{x,z}\right) = 1 \qquad (8)$$

and $$\frac{\partial M}{\partial z} = \frac{\partial \theta}{\partial x} \quad \text{respectively} \qquad (9)$$

Gill noted that eq. (9) may also be expressed in the Jacobian form:

$$J\left(\frac{M,x}{x,z}\right) = J\left(\frac{\theta,z}{x,z}\right)$$

or $$J\left(\frac{M,x}{\theta,z}\right) = 1 \qquad (10)$$

If M and Z (capital used to denote that z differentiation is taken at constant M) are adopted as independent variables then eqs (8) and (10) may be re-expressed as:

$$J\left(\frac{M,\theta}{M,Z}\right) = J\left(\frac{x,z}{M,Z}\right) \qquad (11)$$

and $$J\left(\frac{M,x}{M,Z}\right) = J\left(\frac{\theta,z}{M,Z}\right) \qquad (12)$$

using well-known rules for the products of Jacobians. Eqs (11) and (12) are then simply written as Cauchy-Riemann equations:

$$\frac{\partial \theta}{\partial M} = -\frac{\partial x}{\partial Z} \qquad (13)$$

and $$\frac{\partial \theta}{\partial Z} = \frac{\partial x}{\partial M} \qquad (14)$$



implying that the complex variable $W = x + i\theta$ is an analytic function of $Y = M + iZ$; or $W = W(Y)$ represents a conformal mapping between the W and Y planes. In the physical context of the penetrative convection problem considered here, one particular mapping is of central importance. This is given by:

$$W = \text{Cosh}\,[\text{Sinh}^{-1}(Y)] \qquad (15)$$

and as will be shown later, it has the property that the $\theta = 0$ and $M = 0$ isopleths coincide on a circle in the (x, z) plane. It also has the property that as $|Y| \to \infty$, $W \to Y$ or $M \to x$ and $\theta \to z$ which represents a horizontally stratified atmosphere at rest.

The structure of the solution may be calculated by introducing elliptic coordinates so that:

$$Y = \text{Sinh}\,\zeta \qquad \text{where } \zeta = \alpha + i\beta$$

which implies that:

$$M = \text{Sinh}\,\alpha\,\text{Cos}\,\beta \qquad (16)$$

and $Z = \text{Cosh}\,\alpha\,\text{Sin}\,\beta$ .

Furthermore, eq. (15) can be re-written as:

$$x + i\theta = \text{Cosh}\,(\alpha + i\beta)$$

which on expansion of Cosh and equating real and imaginary parts gives:

$$x = \text{Cosh}\ \alpha\ \text{Cos}\ \beta \qquad (17)$$
$$\theta = \text{Sinh}\ \alpha\ \text{Sin}\ \beta \quad .$$

Note that eqs (16) and (17) imply that M and $\theta$ equal zero on the circle $x^2 + z^2 = 1$ where $\alpha = 0$. The solution will be assumed only to describe the flow outside of this unit circle. Within it we assume that M and $\theta$ are zero so that the interior satisfies the thermal wind equation (9) but has zero potential vorticity. The isentropes and v field corresponding to this solution are depicted in Fig. 3 (a) and (b) respectively.

This circular lens (though elliptical in dimensional (x, z) space) may be thought of as having been produced by the injection of fluid with M and $\theta = 0$ into a horizontally-stratified atmosphere at rest, without mixing. For convective and inertial stability the lens must be centred on the origin.

In the thought experiment envisaged here, the injection of lens fluid corresponds to the arrival at the origin of fluid from a non-entraining two-dimensional convective plume as illustrated schematically in Fig. 4. In the atmospheric context, air arriving in the lens from below is assumed to have suffered internal mixing so as to homogenize the $\theta$ and M fields. The mass flux in this convective plume is imagined to emanate from an initially saturated region of the horizontally-stratified atmosphere at rest. The complementary problem to the homogeneous intrusion therefore concerns the mass sink from whence the convective plume originated. What is the



equilibrium configuration corresponding to the removal of a certain volume of fluid under the assumption of no mixing and two-dimensionality? A special case of some interest is represented by the conformal mapping to be discussed in the following section.

(b) The discontinuity mapping

Consider the following conformal mapping:

$$W = {}^1/_2 \{Y + \sqrt{Y^2 - D^2}\} \qquad (18)$$

where D is a real constant. For large $|Y|$ it can be seen that $W \sim Y$ so that the solution tends to the basic state as in the previous example. The square root term requires the definition of a branch cut on the real axis of the Y-plane which will be taken here to join the branch points at $Y = \pm D$, (Fig. 5). Computation of corresponding points in the W and Y planes is facilitated by the introduction of polar coordinates about the branch points, as in Fig. 5, so that:

$$Y - D = r_1 \exp(i\lambda_1)$$
$$\text{and}\quad Y + D = r_2 \exp(i\lambda_2) \quad \text{with} \quad -\pi < \lambda_2 < \pi$$

Eq. (18) may then be written as:

$$x + i\theta = {}^1/_2 [M + iZ + \sqrt{r_1 r_2} \cdot \{\text{Cos}\ {}^1/_2 (\lambda_1 + \lambda_2) + i\ \text{Sin}\ {}^1/_2 (\lambda_1 + \lambda_2)\}]$$

which, on equating real and imaginary parts, gives:

$$x = {}^1/_2 \, [M + \sqrt{r_1 r_2} \, \text{Cos} \, {}^1/_2 \, (\lambda_1 + \lambda_2)] \qquad (19)$$

$$\theta = {}^1/_2 \, [Z + \sqrt{r_1 r_2} \, \text{Sin} \, {}^1/_2 \, (\lambda_1 + \lambda_2)] \qquad (20)$$

Consider now the variation of $\theta$ along the $z = 0$ axis for the following three cases:

(i) $|Y| > D$

(ii) $|Y| < D$, above the branch cut

(iii) $|Y| < D$, below the branch cut.

For case (i) ${}^1/_2 \, (\lambda_1 + \lambda_2)$ will be $\pi$ (above M-axis on negative side), $-\pi$ (below M-axis on negative side) or 0 (on positive M-axis) all implying $\theta = 0$. Case (ii) requires that:

$$\lambda_1 = \pi \text{ and } \lambda_2 = 0$$

$$r_1 = D - M \text{ and } r_2 = D + M$$

which in eq. (2) gives:

$$\theta = + {}^1/_2 \, (D^2 - M^2)1/2 \qquad (21)$$



On the other hand, case (iii) requires that:

$$\lambda_1 = -\pi \qquad \lambda_2 = 0$$

$$r_1 = D - M \qquad r_2 = D + M$$

so that:

$$\theta = - {}^1/_2 \, (D^2 - M^2)^{1/2} \, . \qquad (22)$$

By the same considerations using eq. (19):

(i) $x = {}^1/_2 \, [M - (M^2 - D^2)^{1/2}]$ $\quad z = 0, \quad M < -D$

$x = {}^1/_2 \, [M + (M^2 - D^2)^{1/2}]$ $\quad z = 0, \quad M > D$

(ii) $x = {}^1/_2 \, M$

and (iii) $x = {}^1/_2 \, M$. The branch cut therefore represents a horizontal discontinuity line of length D in (x, z) . The $\theta$ and M fields have been computed from eqs (19) and (20) and are depicted in Figs 6 (a) and (b). The accompanying geostrophic wind v (= M-x) (Fig. 6 (c)) shows the vorticity to be cyclonic near the discontinuity.

Eqs (21) and (22) describe the $\theta$ - M relation around the discontinuity and represents an ellipse whose equation is:

$$4\,\theta^2 + M^2 = D^2$$

Within this ellipse are values of (M, $\theta$) that are 'missing' in physical space. To create from a horizontally-stratified atmosphere, a flow field whose structure is given by eq. (18), fluid must be removed from the region of physical space corresponding to this region in (M, $\theta$) space (ie within the ellipse ($4\,z^2 + x^2 = D^2$). The fluid particles at the boundary of this ellipse would converge onto the discontinuity line on removal of the fluid.

A variant on the discontinuity mapping (eq. (18)) can be obtained by noting that z + iM is an analytic function of $\theta$ + ix and by writing:

$$z + iM = F\,(\theta + ix)$$

where $F(Y) = {}^1/_2\,[Y + \sqrt{Y^2 - D^2}]$ as before.

It is easily seen that this mapping gives a vertical discontinuity line across which M is discontinuous rather than $\theta$, (Figs 7 (a)-(c)). The $\theta$-M relation on the discontinuity line is now given by:

$$4\,M^2 + \theta^2 = D^2$$



which is an ellipse with major axis along the $\theta$-axis. Therefore, depending on the orientation of the major axis of the elliptical region from which fluid is extracted, one may get a horizontal or vertical discontinuity (Note: the scale of the vertical axis is f/N times that of the horizontal axis in physical space).

The lens and discontinuity mappings therefore constitute the mass source and sink required to describe convection as a forced mass transfer process. The two solutions are exact if treated separately though are only approximate when combined: the degree of approximation depends on how close the lens and discontinuity are. A 'joint' mapping having the property of simultaneously representing a homogeneous lens together with a discontinuity has not been found. Fig. 8 shows the potential temperature field obtained by superposing the lens and vertical discontinuity solutions so that the lens has a potential temperature of 9 units compared to zero in the isolated case of (a). This represents the equilibrium state after air within the half-ellipse ($4\,x^2 + z^2 = D^2$, $z > 0$) has convected 9 non-dimensional height units in the vertical whilst homogenising M and $\theta$ in the process. Obviously, the area of the half-ellipse must equal the area of the lens to be consistent with the continuity equation. D has been chosen so as to enforce this constraint.

## 3. Slantwise convection

### (a) Lens in a uniformly-sheared flow

The foregoing convection problem can also be analysed in a 'baroclinic' environment of uniform potential vorticity. In this context M conservation causes convection to orient itself quasi-horizontally (slantwise convection)and is relevant to the mode of ascent that takes place at cold fronts.

The Cauchy-Riemann equations (13) and (14) may be generalised so that:

$$\frac{\partial}{\partial M}(a\theta + bM) = -\frac{\partial}{\partial Z}(ax - bz) \qquad (23)$$

$$\text{and} \quad \frac{\partial}{\partial Z}(a\theta + bM) = \frac{\partial}{\partial M}(ax - bz) \qquad (24)$$

(where a and b are constants)

implying a conformal mapping:

$$M + iZ = F[(ax - bz) + i(a\theta + bM)]$$

$$\text{or} \quad Z + iM = F[(a\theta + bM) + i(ax - bz)] \qquad (25)$$



The basic state corresponding to the mapping F(W) = W gives:

$$a\theta + bM = z$$

and $ax - bz = M$

from which one can infer that:

$$\theta = z\,\frac{(1 + b^2)}{a} - bx \qquad (26)$$

$$\text{and} \quad v = M - x = (a - 1)x - bz \qquad (27)$$

A homogeneous lens of fluid embedded in this flow is given by the mapping:

$$ax - bz + i\,(a\theta + bM) = \text{Cosh}\,[\text{Sinh}^{-1}(Y)]$$

with $Y = M + iZ$. Again using elliptical coordinates $\alpha$ and $\beta$ such that:

$$Y = \text{Sinh}\,(\alpha + i\beta)$$

it is easily shown that:

$$M = \text{Sinh}\,\alpha\,\text{Cos}\,\beta \qquad Z = \text{Cosh}\,\alpha\,\text{Sin}\,\beta \qquad (28)$$

$$ax - bz = \text{Cosh}\,\alpha\,\text{Cos}\,\beta \quad \text{and} \quad a\theta + bM = \text{Sinh}\,\alpha\,\text{Sin}\,\beta\,.$$

When $\alpha = 0$, eqs. (28) gives:

$$M = 0 \qquad Z = \sin\beta$$

$$ax - bz = \cos\beta \quad \text{and} \quad a\theta + bM = 0$$

from which it can be deduced that $\theta$ and M are zero on the ellipse $(ax - bz)^2 + z^2 = 1$. Figs 9 (a) and (b) show the potential temperature and geostrophic wind in the vicinity of the lens when $a = 1$, $b = -1$.

(b) Frontal discontinuity

Returning to the discontinuity mapping $F(W) = {}^1/_2[W + \sqrt{W^2 - D^2}]$ where W now equals $(a\theta + bM) + i\,(ax - bz)$, eq. (25) implies branch points at $a\theta + bM = \pm 1$ with $ax - bz = 0$ on the branch cut (the equation of the frontal discontinuity). When $(a\theta + bM)^2 > D^2$, and $ax - bz = 0$ eq. (25) gives:

$$z = {}^1/_2\,[a\theta + bM + \sqrt{(a\theta + bM)^2 - D^2}]$$

and $M = 0$

which implies that:

$$z = {}^1/_2\,[a\theta + \sqrt{(a\theta)^2 - D^2}] \ .$$



Along the frontal discontinuity where $(a\theta + bM)^2 < D^2$ and $ax - bz = 0$, eq. (25) gives:

$$z = {}^1/_2\,(a\theta + bM) \tag{29}$$

and $$M = \pm {}^1/_2 \sqrt{D^2 - (a\theta + bM)^2} = \pm {}^1/_2 \sqrt{D^2 - 4z^2} \tag{30}$$

where the sign depends on whether one is above or below the branch cut. The ends of the discontinuity line are located at the points

$\left(\frac{bD}{2a}\ ,\ \frac{D}{2}\right)$ and $\left(\frac{-bD}{2a}\ ,\ \frac{-D}{2}\right)$ in the (x, z) plane

The $\theta$-M relation around the discontinuity is given by eqs. (29) and (30) and can be written as:

$$4M^2 + (a\theta + bM)^2 = D^2$$

Since $a\theta + bM = z$ and $ax - bz = M$ initially and M and $\theta$ are conserved outside of this ellipse in (M, $\theta$) space then the fluid to be removed by convection is contained within the ellipse:

$$4\,(ax - bz)^2 + z^2 = D^2 \tag{31}$$

By adopting a polar coordinate representation about each branch point in the (aθ + bM, ax - bz) plane as in section 2(b),it is possible to find sets of points (x,z,M,θ) which satisfy the conformal mapping equation. In this way a search can be performed numerically to find certain θ or M values and plot their isopleths in the (x,z) plane. Fig. 10(a) and (b) show the resulting θ and v contours for the frontal discontinuity with a = 1, b = -1.

θ and v are both discontinuous across the 'front' and Margules' formula is satisfied there. To show this we note that the equation of the front is ax - bz = 0 giving a slope of a/b. Now, eq. (29) implies that aθ + bM is continuous across the front or

$a[\theta] + b[M] = 0$. This can be written as the non-dimensional form of Margules' equation:

$$\frac{dz}{dx} = \frac{a}{b} = -\frac{[M]}{[\theta]}$$ so that [θ] and [M] are consistent with the frontal slope a/b.

A convenient property of this mapping is that the quantity aθ + bM is equal to zero at z = 0 in the basic state and in the discontinuity solution. Since θ and M are conserved in our thought experiment, fluid initially at z = 0 will remain there after the elliptical region of fluid given by eq. (31) is removed. Therefore, as in the upright convection cast, it is permissible to think of z = 0 as a rigid surface (or the 'ground') and only consider the removal of the corresponding upper half ellipse of fluid, (Fig. 11).



The lens and discontinuity solution may now be put together as an 'after state' by assigning a value of θ to the lens fluid (say, $\theta_*$). If the lens and discontinuity are sufficiently well separated the two perturbation responses may be linearly superposed in physical space giving a potential temperature field as in Fig. 12.

These analytic solutions suggest that slantwise convection embedded in a zone of enhanced temperature gradient could create a front (as a surface of discontinuity extending from the ground) on the time scale of the convective mass transfer itself. Such issues will be discussed more fully in Section 4.

c. Mass displacement

Since M and θ are conserved during the mass adjustment from the initial to final state it is possible to calculate the vector displacement field required for the geostrophic adjustment of the non-convecting fluid. Fig. 13 shows the displacement vectors for the upright convection case portrayed in Fig. 8. Fluid on the half-ellipse ($4x^2 + z^2 = D^2$, $z > 0$) in the initial state converges on to the upright discontinuity line. Mesoscale descent is also forced over a horizontal scale of the Rossby radius of deformation based on the thickness of the lens. As before displacement vectors of the two separate analytic solutions have been added implying a small (though negligible) error.

Displacement vectors have also been obtained for the slantwise convection case corresponding to Fig. 12 and show the preference for mesoscale descent along the basic state M surfaces, (ie. opposite to the direction of slantwise ascent by the convecting fluid) (Fig. 14). In both this solution and the upright convection case, mesoscale ascent occurs above the lens with a maximum in the M surface which intersects the lens. The displacement vectors associated with the convection itself are not shown.

## 4. Discussion

The analytic solutions of Section 2 and 3 represent the geostrophic and hydrostatically balanced equilibrium states attained after an absolute momentum conserving rearrangement of mass is brought about by convection. The whole process may be regarded as an extreme example of the geostrophic adjustment problem studied by Rossby (1938) and reviewed by Charney (1973) and Blumen (1972). Conservation of potential temperature, absolute momentum and potential vorticity in the 'environment' fluid coupled with known values for the potential temperature, absolute momentum and mass of the homogeneous fluid which has undergone convection, uniquely determines a final equilibrium state. In the thought experiment envisaged here, a two-dimensional basic state atmosphere with uniform potential vorticity is imagined to contain a saturated elliptical region in a state of unstable equilibrium with respect to buoyancy generated by latent heat release. This region of saturated air convects to its new equilibrium position on the assumption that internal mixing homogenizes the absolute momentum and potential temperature. Before the convection takes place the saturated air



has convective available potential energy (CAPE). In the limit of an infinitesimal mass of saturated air, the CAPE is equal to the positive area between the environment and parcel curves on a tephigram in the usual sense. If a finite volume of air convects so that its volume-averaged thermodynamic state variables follow the same path on the tephigram as the infinitesimal parcel, then a certain fraction of the work done by the buoyancy force is expended on adjusting the environment into a new state of thermal wind balance. All of the kinetic energy released during the ascent of an infinitesimal parcel during convection is ultimately lost through the radiation of internal gravity waves and viscous dissipation. On the other hand, a finite convective mass transfer will lead to the creation of a balanced wind field in the vicinity of the level of no buoyancy and less energy will be radiated away as gravity waves, (Charney, 1973). Of course, these are properties of convection in a rotating system; without rotation isentropic surfaces are horizontal in the equilibrium state and the problem reduces to the vertical column model of Section 1 with continuous stratification.

The treatment of convection as a forced mass transfer process has also been investigated by Gill et al (1979) in the context of bottom water creation by surface cooling of the Greenland sea. Their model was axisymmetric and composed of two homogeneous fluids representing well-mixed and deep water layers. The effect of surface cooling was mimicked by the instantaneous conversion of well-mixed water to deep water thereby creating an effective mass sink in the upper layer and a source in the lower layer. Conservation of angular momentum in the process then demands that a cold

dome of bottom water should form with anticyclonic rotation. Convergence in the upper layer creates cyclonic relative vorticity analogous to that in the discontinuity solutions given here.

The forced mass transfer models of upright and slantwise convection given here are clearly very idealised and are not amenable to quantitative comparison with observations. For instance, evaporational cooling of air into which precipitation is falling is an important effect which would make a substantial impact on the type of equilibrium structure that might result after convection - particularly for upright convection. Mixing and surface/boundary layer friction are also likely to modify the structure of the 'after-state' in a quantitatively important manner, though to what extent is not known. It should be remembered that the solutions given here are two-dimensional and therefore the upright convection solution only makes sense in the context of squall lines and the geostrophically-balanced state accompanying them.

With these restrictions in mind, we note that a familiar feature of tropical squall lines is the appearance of a mesoscale downdraught underneath the cirrus anvil and the descent of mid-tropospheric air to the surface. (Zipser, 1968; Houze, 1977). Whilst this is in part due to evaporational cooling of precipitation into air below the anvil, Miller and Betts (1977), showed that the descent could be dynamically induced on the mesoscale (100-500 km) consistent with our forced mass transfer picture. Even so, it is not clear how realistic the lens model of the convective



after-state is, particularly since the geostrophic adjustment time would be of the order of one day at the latitude of the squall lines in the Houze study.

The slantwise convection after-states of Section 3 are more likely to be of physical relevance since the two-dimensionality requirement is naturally imposed by the straightness of the flow in frontal zones. The solutions suggest that a front could develop in a baroclinic zone on the time scale of slantwise convective mass transfer even in the absence of deformation by the synoptic scale flow. This would happen as a finite mass of moist saturated air initially in contact with the ground ascends to a new convectively stable position along the relevant M surface. The vacated space is filled in such a way that air parcels with different absolute momenta are brought into contact at a frontal discontinuity line extending from the surface. Subsidence tends to occur along the M surfaces of the basic state except near to the lens or discontinuity. Ascent is forced further up the M surface which intersects the lens.

Unfortunately, support for this picture is very difficult to infer from existing observational studies of frontal circulation for a variety of reasons. Apart from the natural richness of detail in observed fronts associated with the confluence of airstreams of varied origin, slantwise convection must be expected in frontogenetic zones where ageostrophic circulations already exist. Therefore, Fig. 12 could be regarded as the component of the ageostrophic velocity field associated with continuous slantwise convection embedded in a developing front. Since the classical dry model of a front (Hoskins and Bretherton, 1972) involves ascent in the

warm air and descent in the cold air, the superposition of this ageostrophic circulation due to slantwise convection implies weakened ascent in the warm air and strengthened descent in the cold air. The slantwise convection itself could be thought of as a narrow plume of rapidly ascending air joining the lens to the discontinuity. Emanuel et al (1987) have shown that in a two-dimensional Eady wave model in which all ascent (descent) is saturated (unsaturated), the scale of the ascent decreases to zero as the moist potential vorticity (based on the equivalent potential temperature) tends to zero. This limit is equivalent to allowing the stability measured in absolute momentum surfaces to tend to zero. From this viewpoint their results support the 'plume' mode of ascent envisaged here though strictly speaking the model presented in this paper gives no explicit information about this.

The case study of Ogura and Portis (1982) provides some observational support for a shallow ascending plume of boundary layer air embedded within a region of descent. In a frontal zone containing vigorous convection they found descent and an associated cloud-free zone ahead of the surface cold front and rapidly sinking cold air behind the front. In less extreme convective situations where the mode of ascent is still convective but slantwise, one might expect weak ascent in the warm air and strong descent in the cold air.

These speculations lead us to a very important question concerning the dynamical nature of the ascent at cold fronts. That is, 'Can slantwise convection proceed as a quasi-steady component of frontal motion or does the ascent occur under weak slantwise stability? (Thorpe and Emanuel



(1985)). Although both processes could be under the control of synoptic-scale dynamical forcing (eg geostrophic deformation) the former mode of behaviour releases slantwise convective available potential energy (Emanuel, 1983) from the system and could give rise to a qualitatively different type of response to that when the slantwise stability is positive. Furthermore,it is not clear what might happen to the unbalanced kinetic energy released in slantwise convection. It could be dissipated locally in turbulence and/or radiated in inertial gravity waves during the geostrophic adjustment process or a substantial proportion of it might be injected into the balanced flow (eg the jetstream) as a kind of organised convective momentum transport. This would necessarily involve a three-dimensional motion field in which absolute momentum was not conserved following the motion of air parcels. Green et al (1966) suggested that Trade wind boundary layer air could ascend to the upper troposphere at cold fronts in mid-latitude weather systems and that the speed of the jetstream into which the air is injected could be related to the release of potential energy along the trajectory (see also Betts and McIlveen, 1969 for an important correction to their analysis). Their theory supposes frictionless ascent without any energy being lost in the geostrophic adjustment process in contrast that predicted by the simple models given here.

The level of energy loss associated with convection could have an important bearing on the evolution of baroclinic weather systems and hence the weather forecasting problem.

The analytic solutions of Sections 2 and 3 are obviously very special cases of balanced solutions before and after convection and only provide an idealised picture of the type of response one might obtain for more realistic initial flow states. Solutions for general piecewise constant data can be obtained using the geometric algorithm described in Cullen et al (1987) and illustrated by the example in the Introduction. In the dry case, their technique involves rearranging a finite number of parcels or elements into a symmetrically stable equilibrium state whilst holding constant their absolute momentum and potential temperature and is based on theorems given by Cullen and Purser (1984). The method can be extended to the moist case by rearranging all unsaturated parcels at constant potential temperature and all saturated parcels at constant equivalent temperature. On saturating, some parcels may convect to a higher level depending on the environment curve they 'see' on a tephigram plotted at constant M. Details of this method and some applications will appear elsewhere in the literature.

## 5. Summary

Analytic solutions have been obtained which describe the two-dimensional balanced state of the atmosphere after an idealised form of convection has taken place. This convection involves the transfer of a certain mass of fluid from its initial undisturbed position to a level of neutral buoyancy whilst conserving absolute momentum. The fluid is assumed to internally mix during the convection but causes no entrainment. In the final geostrophic and hydrostatic equilibrium state, the convected fluid occupies a lenticular region of width $N/f$ times its depth. The lens itself



has zero absolute vorticity consistent with the hypothesis of internal mixing of absolute momentum. Fluid at the periphery of the elliptical region of fluid which undergoes convection, pinches together to form an internal discontinuity in the balanced, final state. When convection takes place in an atmosphere with a pre-existing horizontal temperature gradient, a front is formed. Since the parcel's absolute momentum is conserved this is simply slantwise convection. The solutions suggest a zone of mesoscale forced descent about the M surface corresponding to the absolute momentum of the convecting parcel.

A fundamental question brought into focus by this work is, 'To what extent is the non-entraining model of slantwise convection valid? Since it is still not clear how prevalent slantwise convection is in real atmospheric fronts, this question, along with many other must await observational field studies with high spatial resolution.

Acknowledgementsa

I would like to thank Mike Booth for producing the computer-plotted Figures and Martin Holt for the element model calculation described in the Introduction.

Figures

1. Vertical fluid column comprising of five elements with uniform potential temperature:
   (a) before heating element 1
   (b) After heating " "

2. (a) Initial element representation of a stratified fluid at rest.
   (b) New geostrophically adjusted state after an impulse of heat is supplied to element 30.

3. Gill's homogeneous intrusion in non-dimensional (x, z) space.
   (a) $\theta$.
   (b) v. contour interval: 0.04

4. Schematic diagram illustrating the convective mass transfer thought experiment.

5. Complex plane of Y indicating the branch cut and polar coordinate representation about each branch point.

6. Isolated horizontal discontinuity solution with D=1. Contours for:
   (a) $\theta$. Contour interval: 0.5
   (b) M. Contour interval: 1.0
   (c) v. Contour interval: 0.1



7. Isolated vertical discontinuity solution with D=1. Contours for:
   (a) $\theta$. Contour interval: 0.125
   (b) M. Contour interval: 0.25
   (c) v. Contour interval: 0.1

8. Superposition of the lens and vertical discontinuity solution choosing D=2 for compatibility between the mass removed and lens volume. Contour interval: 0.15.

9. Lens solution in a uniform baroclinic zone with a = 1, b = -1.
   (a) $\theta$. Contour interval: 0.5
   (b) v. Contour interval: 0.2

10. Frontal discontinuity solution with a = 1, b = -1.
   (a) $\theta$. Contour interval: 0.4
   (b) v. Contour interval: 0.2

11. Initial state (a = 1, b = -1) with $\theta$ (bold lines), M (dashed lines) and half ellipse denoting the fluid involved in convection.

12. Super-position of the lens and discontinuity solutions in a uniform baroclinic zone with a = 1, b = -1 and $\theta_* = 9$. Contour interval: 0.5

13. Displacement vectors corresponding to Fig. 8.

14. Displacement vectors corresponding to Fig. 12.

References

Bennetts, D.A. and Hoskins, B.J. (1979) 'Conditional symmetric instability: A possible explanation for frontal rainbands.' Quart. J. Roy. Met. Soc., 105, 945-962.

Betts, A.K. and McIlveen, J.F.R. (1969) 'The energy formula in a moving reference frame. Quart. J. Roy. Met. Soc., 95, 639-642.

Blumen, W. (1972) 'Geostrophic adjustment'. Rev. Geophys. Space Phys. 10, 485-528.

Charney, J.G. (1973) 'Planetary fluid mechanics'. In Dynamical Meteorology (ed. P. Morel) Reidel.

Cullen, M.J.P., Chynoweth, S. and Purser, R.J. (1987) 'On semi-geostrophic flow over synoptic scale topography'. (accepted, Quart. J. Roy. Met. Soc.)

Cullen, M.J.P. and Purser, R.J. (1984) 'An extended Lagrangian theory of semi-geostrophic frontogenesis'. J. Atmos. Sci., 41, 1441-1497

Emanuel, K. (1983) 'On assessing local conditional symmetric instability from atmospheric soundings'. Mon. Wea. Rev., 111, 2016-2033

Emanuel, K., Fantini, M. and Thorpe, A.J. (1986) 'Baroclinic instability in an environment of small stability to slantwise moist convection. Part 1: Two-dimensional models'. (Submitted to J. Atmos. Sci.)

Gill, A.E. (1981) 'Homogeneous intrusions in a rotating stratified fluid'. J. Fluid Mechs. 103, 275-295.

Gill, A.E., Smith, J.M., Cleaver, P., Hide, R. and Jonas, P. (1979) 'The vortex created by mass transfer between layers of a rotating stratified fluid'. Geophys. Astrophys. Fluid Dyn. 12, 195-220.

Green, J.S.A., Ludlam, F.H. and McIlveen, J.F.R. (1966) 'Isentropic relative flow analysis and the parcel theory'. Quart. J. Roy. Met. Soc., 92, 210-219.

Hoskins, B.J. (1975) 'The geostrophic momentum approximation and the semi-geostrophic equations'. J. Atmos. Sci., 32, 233-242.

Hoskins, B.J. and Bretherton, F.P. (1972) "Atmospheric frontogenesis models: mathematical formulation and solution'. J. Atmos. Sci., 29, 11-37.

Hoskins, B.J. and Draghici, I. (1977) 'The forcing of ageostrophic motion according to the semi-geostrophic equations and in an isentropic coordinate model'. J. Atmos. Sci., 34, 1859-1867.



Houze, R.A. (1977) 'Structure and dynamics of a tropical squall-line system'. Mon. Wea. Rev., 105, 1540-1567.

Miller, M.J. and Betts, A.K. (1977) 'Travelling convective storms over Venezuela'. Mon. Wea. Rev., 105, 833-848.

Ogura, Y. and Portis, D. (1982) 'Structure of the cold front observed in SESAME-AVE III and its comparison with the Hoskins-Bretherton frontogenesis model'. J. Atmos. Sci., 39, 2773-2792.

Riehl, H. and Malkus, J.S. (1958) 'On the heat balance of the equatorial trough zone'. Geophysica, 6, 503-538.

Rossby, C.G. (1938) 'On the mutual adjustment of pressure and velocity distributions in certain simple current systems'. J. Mar. Res., 1, 15-28, 239-263.

Shutts, G.J. and Cullen, M.J.P. (1987) 'Parcel stability and its relation to semi-geostrophic theory (accepted for J. Atmos. Sci.)

Shutts, G.J. and Thorpe, A.J. (1978) 'Some aspects of vortices in rotating stratified fluids'. Pageoph., 116, 993-1006

Thorpe, A.J. and Emanuel, K. (1985) 'Frontogenesis in the presence of small stability to slantwise convection'. J. Atmos. Sci., 42, 1809-1824.

Zipser, E.J. (1969) 'The role of organised unsaturated convective downdraughts in the structure and rapid decay of an equatorial disturbance'. J. Appl. Meteor., 8, 799-814.



Fig. 1

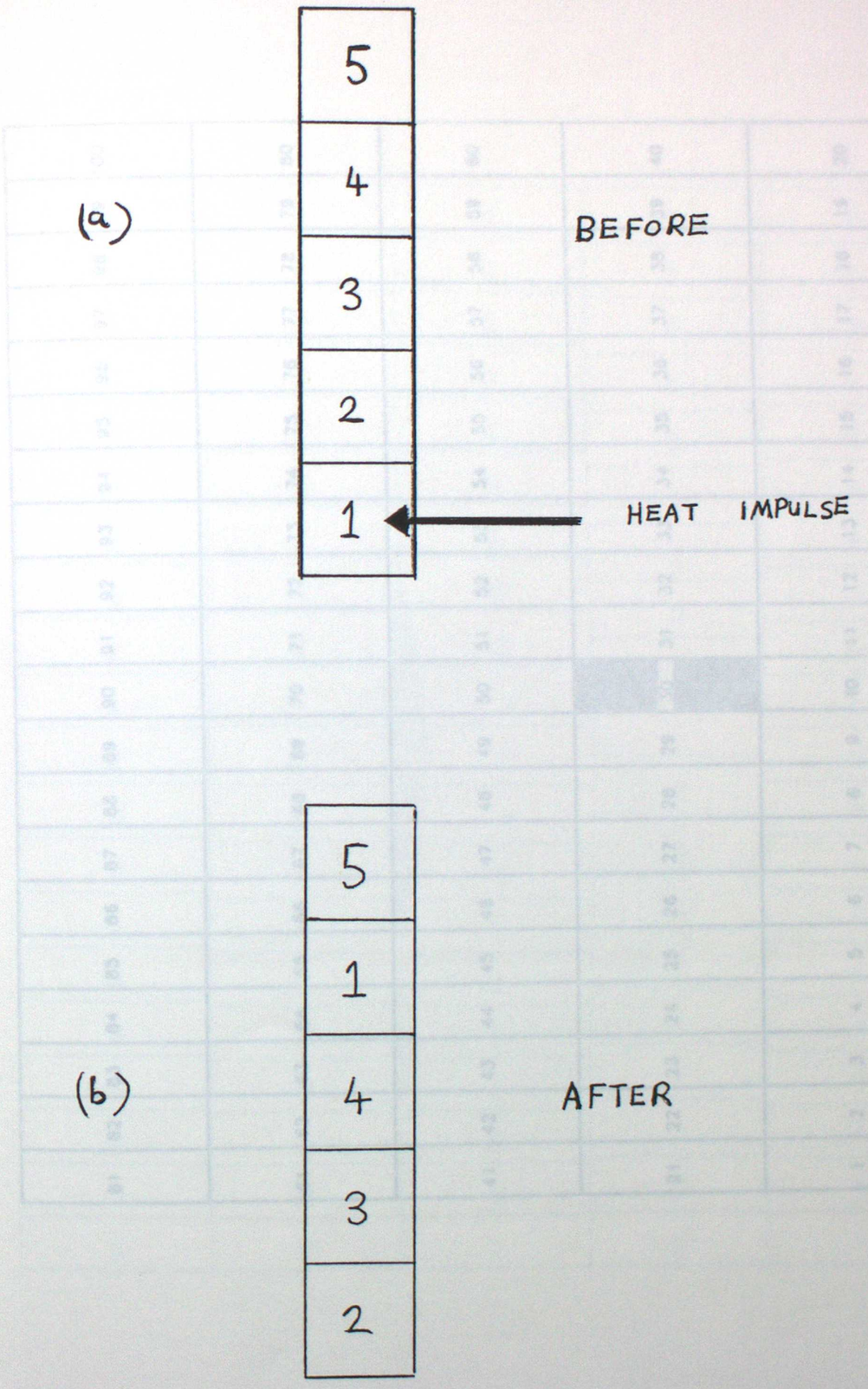

Fig. 2 (a)

| | | | | | | | | | | | | | | | | | | |
|---|---|---|---|---|---|---|---|---|---|---|---|---|---|---|---|---|---|---|
| 81 | 82 | 83 | 84 | 85 | 86 | 87 | 88 | 89 | 90 | 91 | 92 | 93 | 94 | 95 | 96 | 97 | 98 | 99 | 100 |
| 61 | 62 | 63 | 64 | 65 | 66 | 67 | 68 | 69 | 70 | 71 | 72 | 73 | 74 | 75 | 76 | 77 | 78 | 79 | 80 |
| 41 | 42 | 43 | 44 | 45 | 46 | 47 | 48 | 49 | 50 | 51 | 52 | 53 | 54 | 55 | 56 | 57 | 58 | 59 | 60 |
| 21 | 22 | 23 | 24 | 25 | 26 | 27 | 28 | 29 | 30 | 31 | 32 | 33 | 34 | 35 | 36 | 37 | 38 | 39 | 40 |
| 1 | 2 | 3 | 4 | 5 | 6 | 7 | 8 | 9 | 10 | 11 | 12 | 13 | 14 | 15 | 16 | 17 | 18 | 19 | 20 |

Fig. 2 (b)

| | | | | | | | | | | | | | | | | | | | |
|---|---|---|---|---|---|---|---|---|---|---|---|---|---|---|---|---|---|---|---|
| 81 | 82 | 83 | 84 | 85 | 86 | 87 | 88 | 89 | 90 | 91 | 92 | 93 | 94 | 95 | 96 | 97 | 98 | 99 | 100 |
| 61 | 62 | 63 | 64 | 65 | 66 | 67 | 68 | 69 | 70 | 71 | 72 | 73 | 74 | 75 | 76 | 77 | 78 | 79 | 80 |
| 41 | 42 | 43 | 44 | 45 | 46 | 47 | 48 | 49 | 50 | 51 | 52 | 53 | 54 | 55 | 56 | 57 | 58 | 59 | 60 |
| 21 | 22 | 23 | 24 | 25 | 26 | 27 | 28 | 29 | 31 | 32 | 33 | 34 | 35 | 36 | 37 | 38 | 39 | 40 | |
| 1 | 2 | 3 | 4 | 5 | 6 | 7 | 8 | 9 | 10 | 11 | 12 | 13 | 14 | 15 | 16 | 17 | 18 | 19 | 20 |

30

Fig. 3 (a)

Fig. 3 (a)

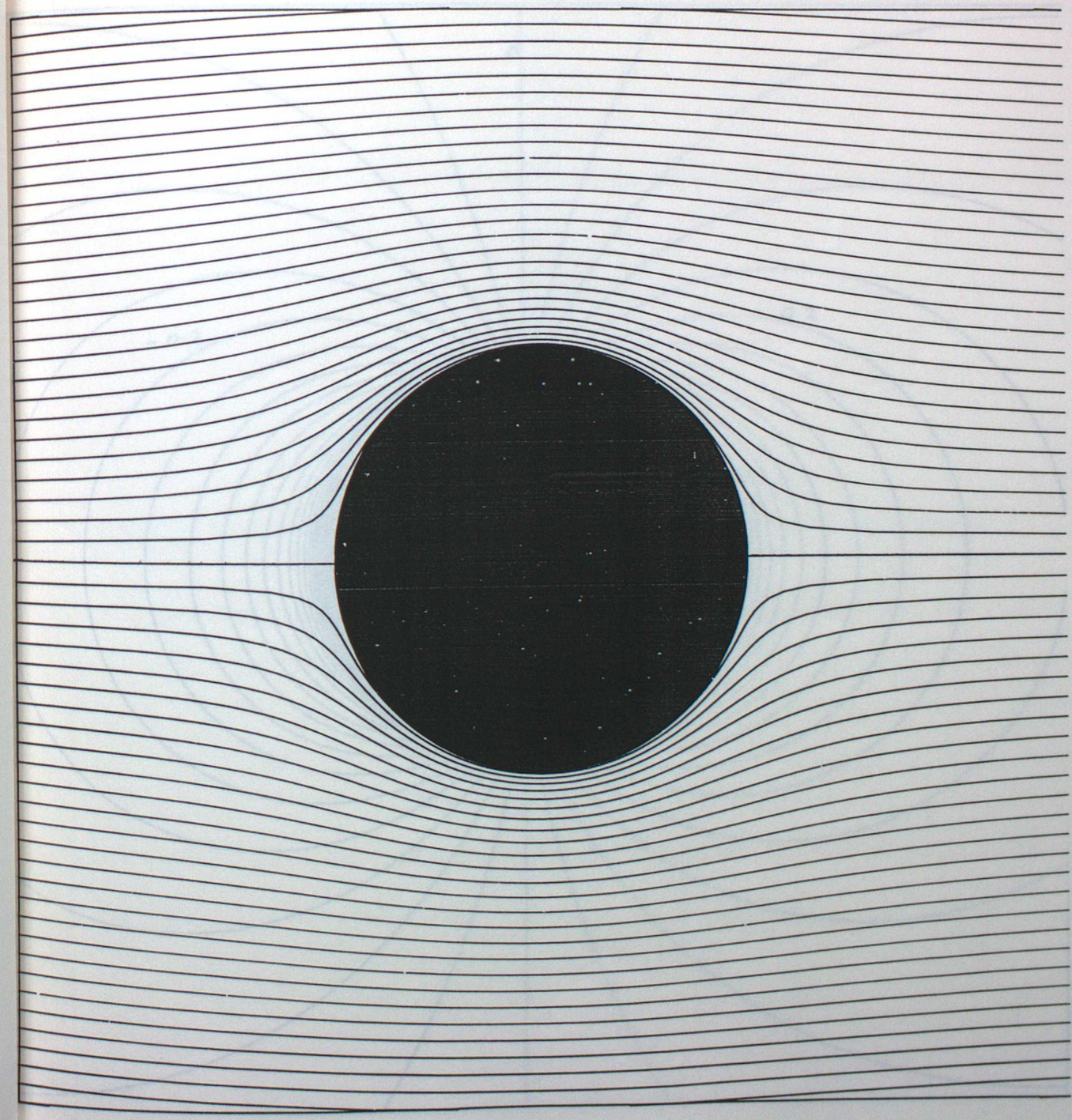

Fig. 3(b)

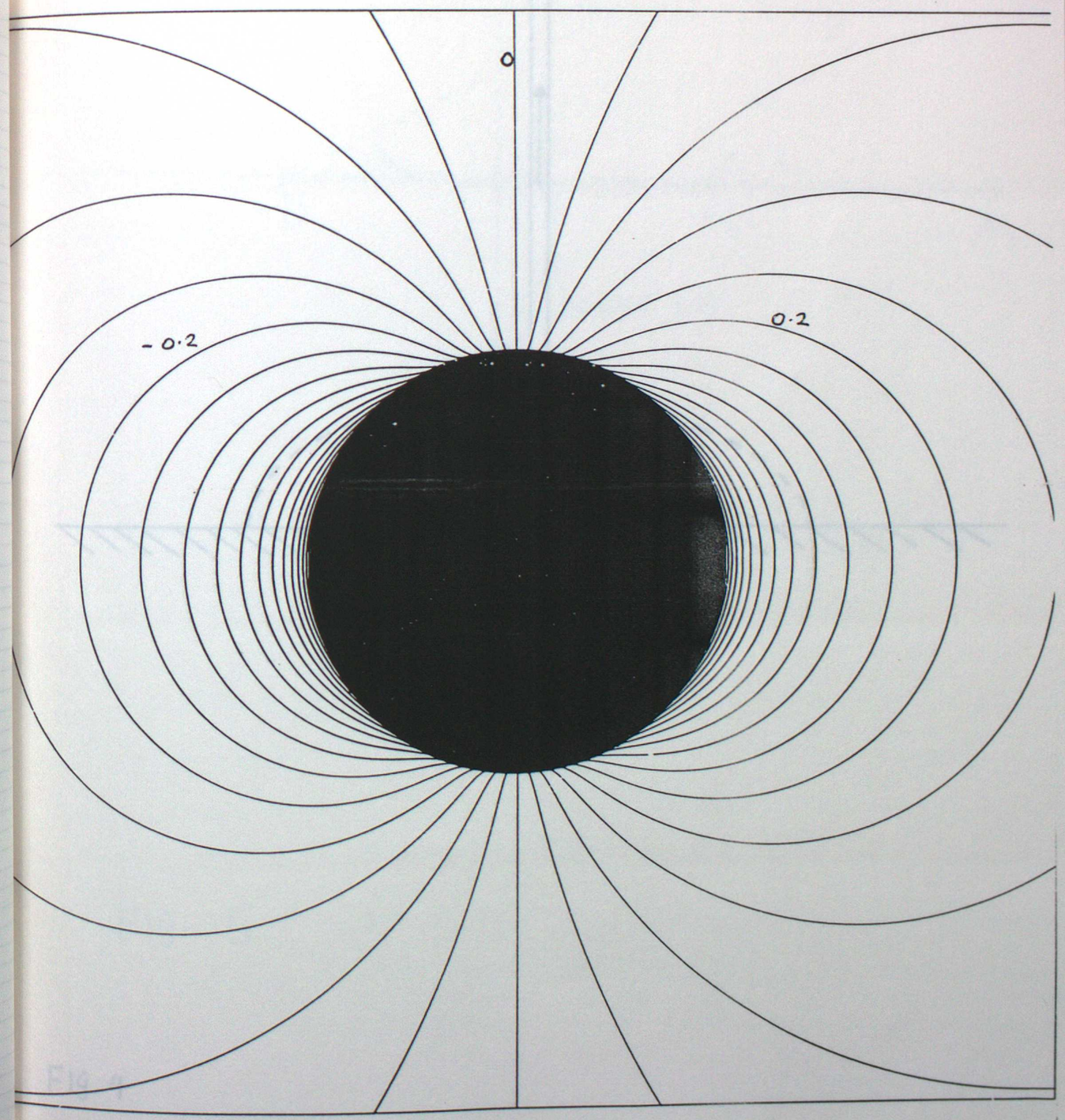

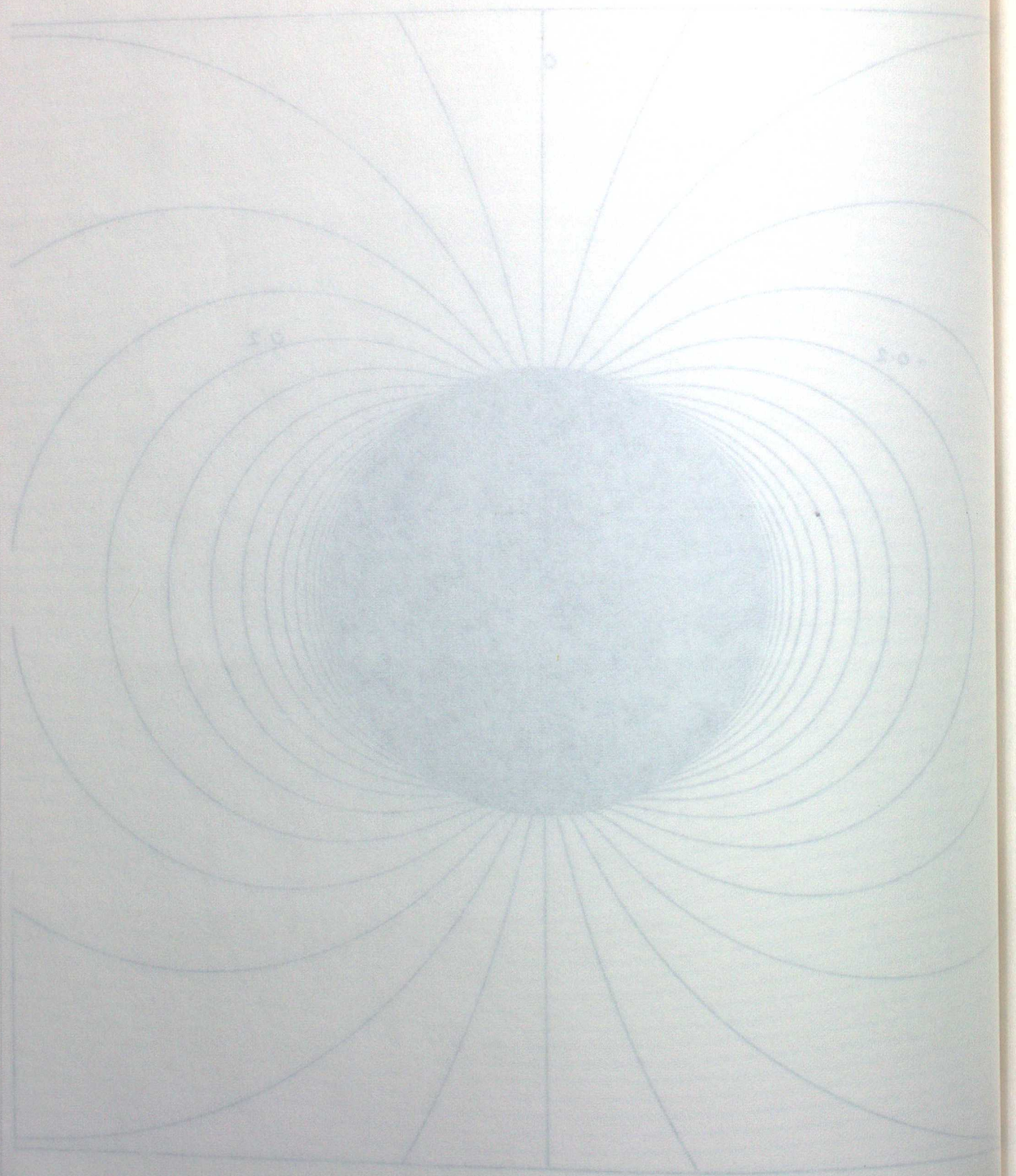

Fig. 4

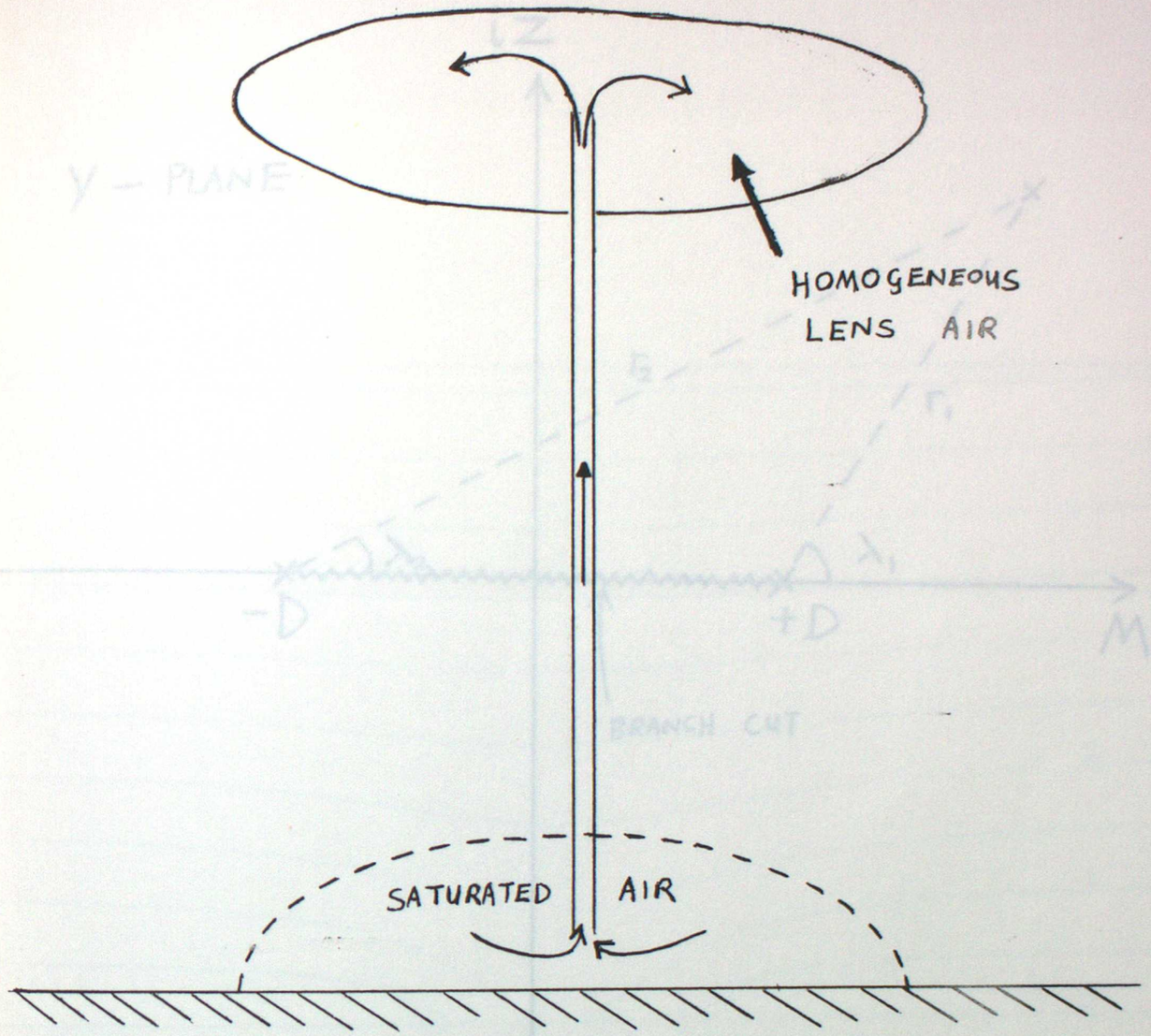


Fig. 5

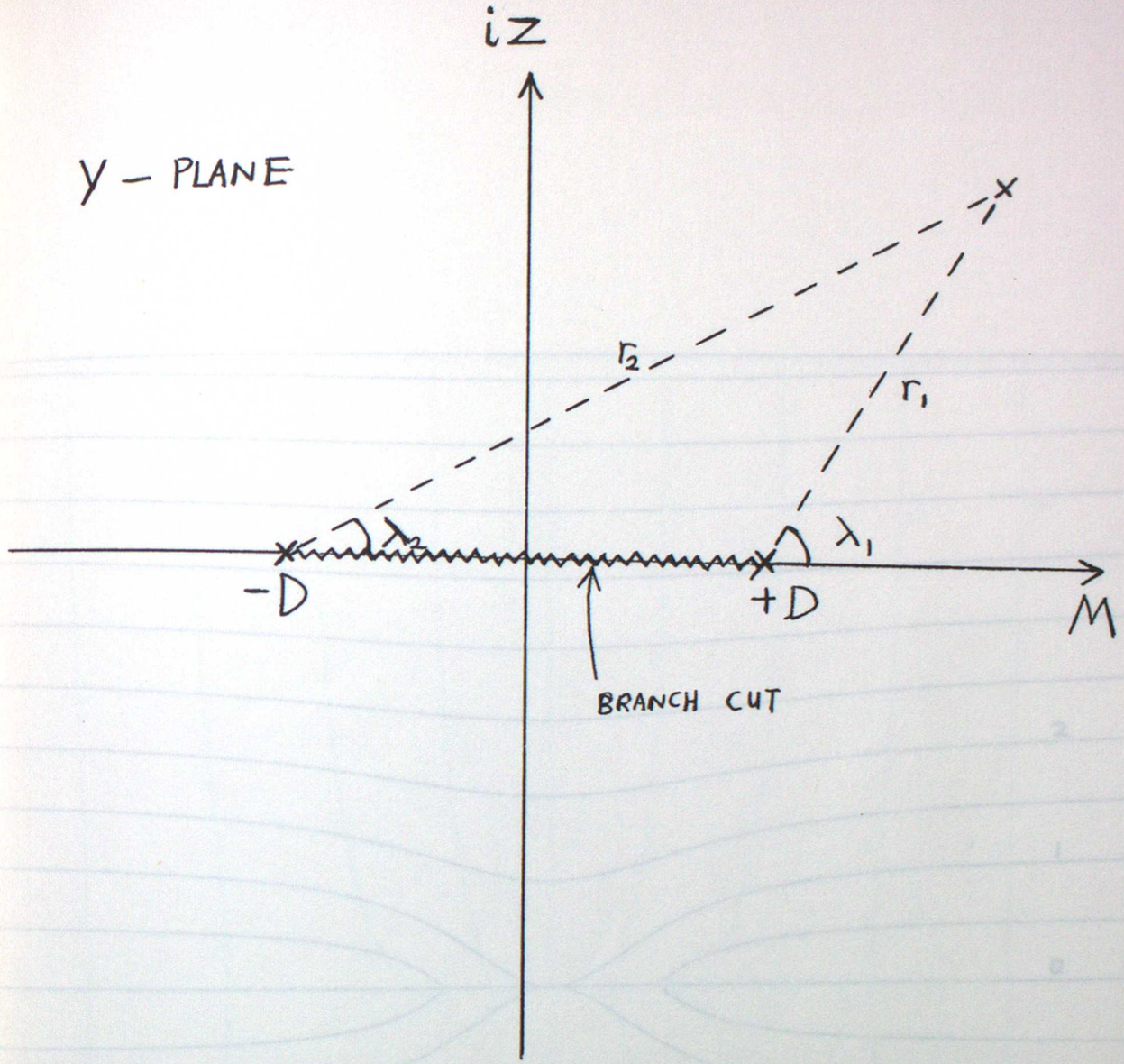


Fig. 5

Fig. 6 (a)

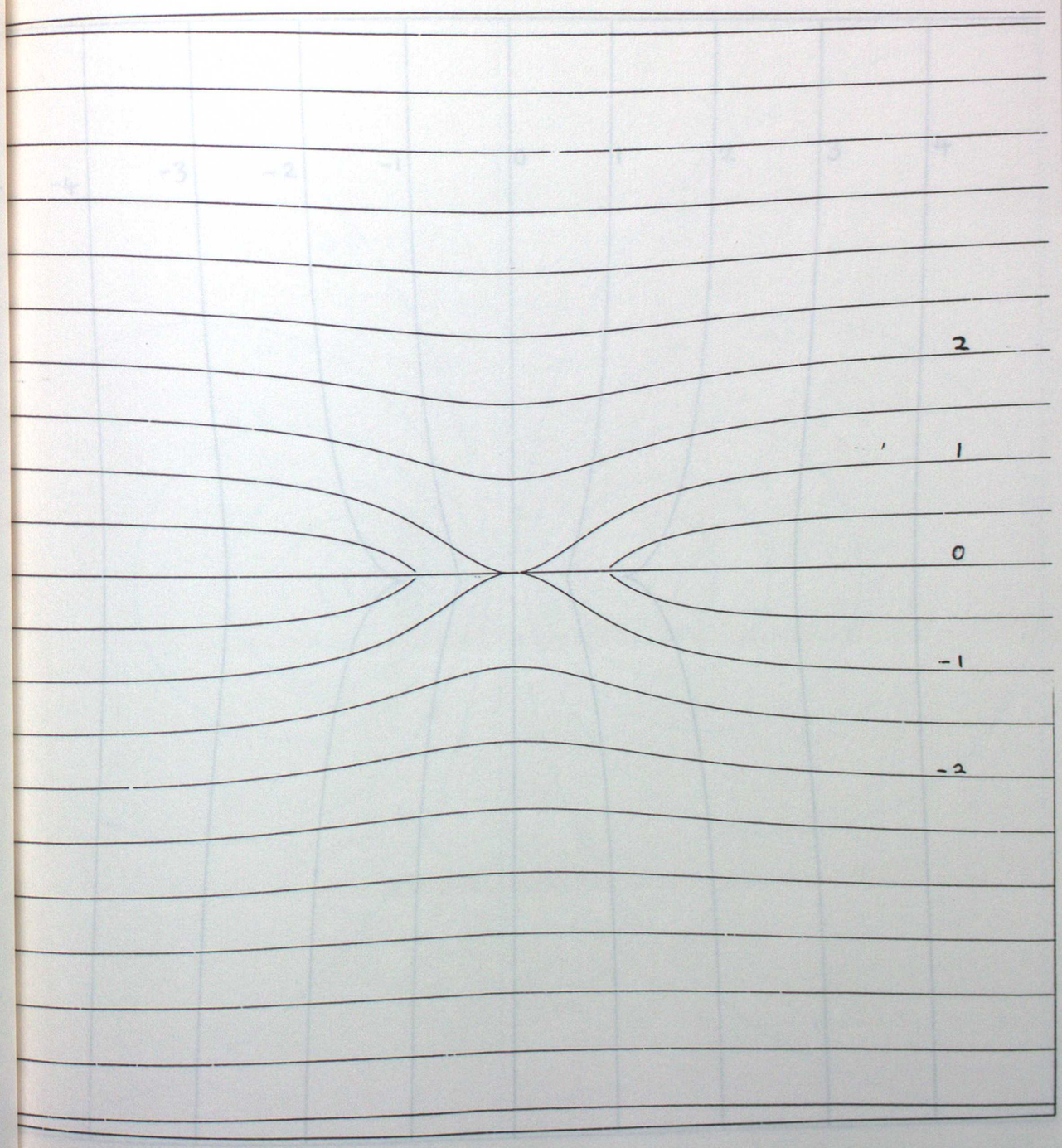

Fig. 6 (b)

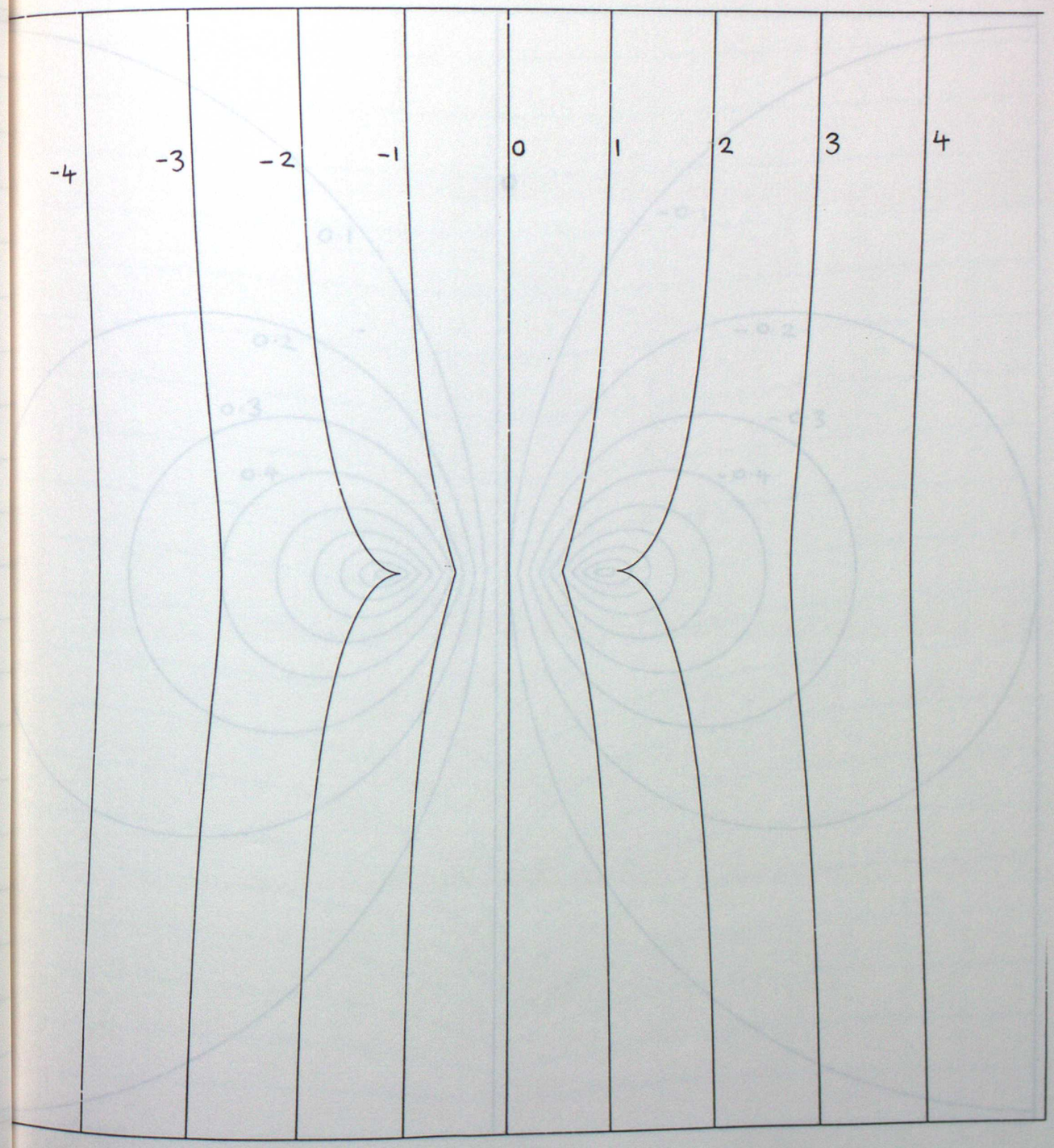

Fig. 6(c)

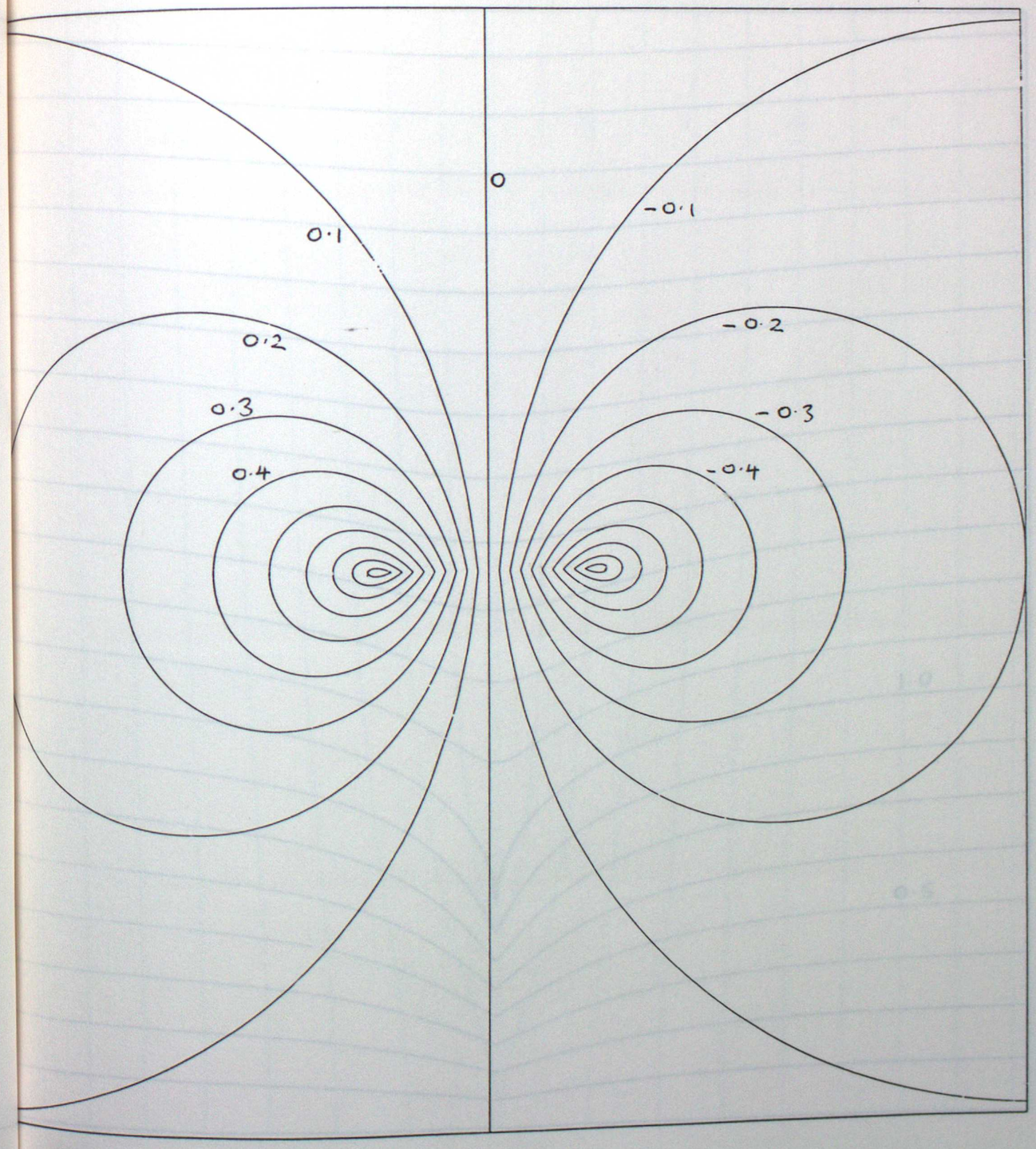

Fig. 7(a)

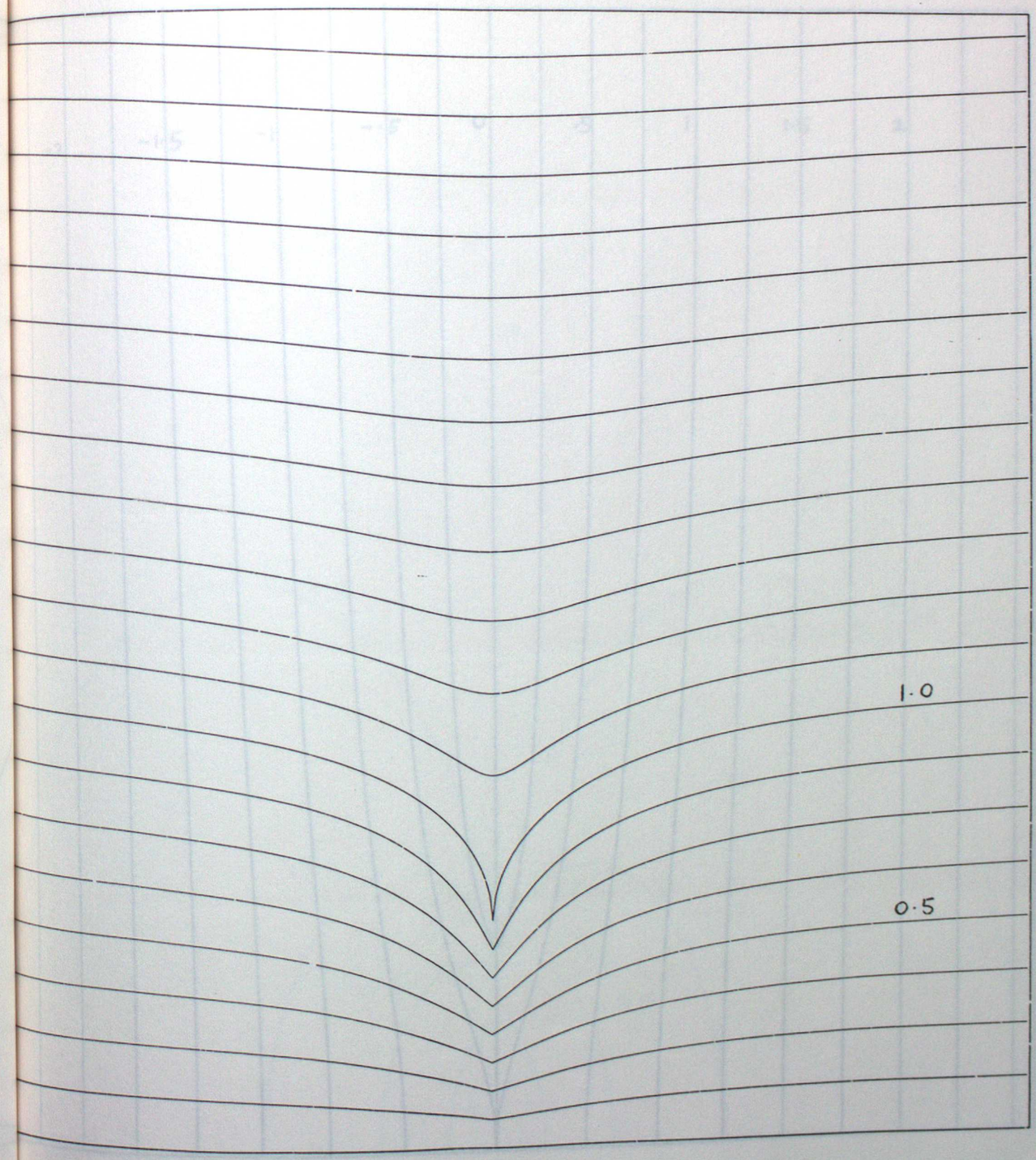

Fig. 7(b)

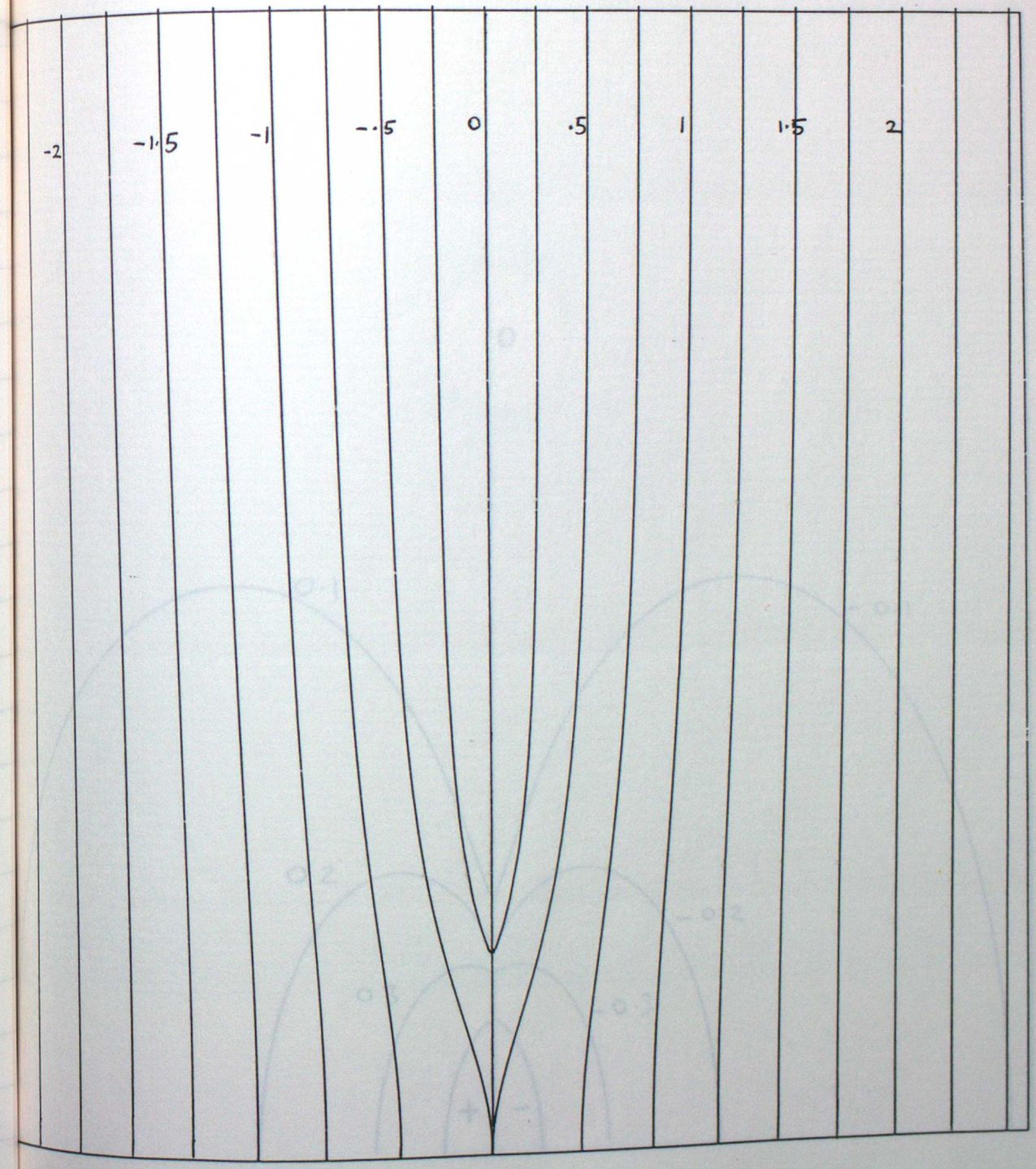

Fig. 7(c)

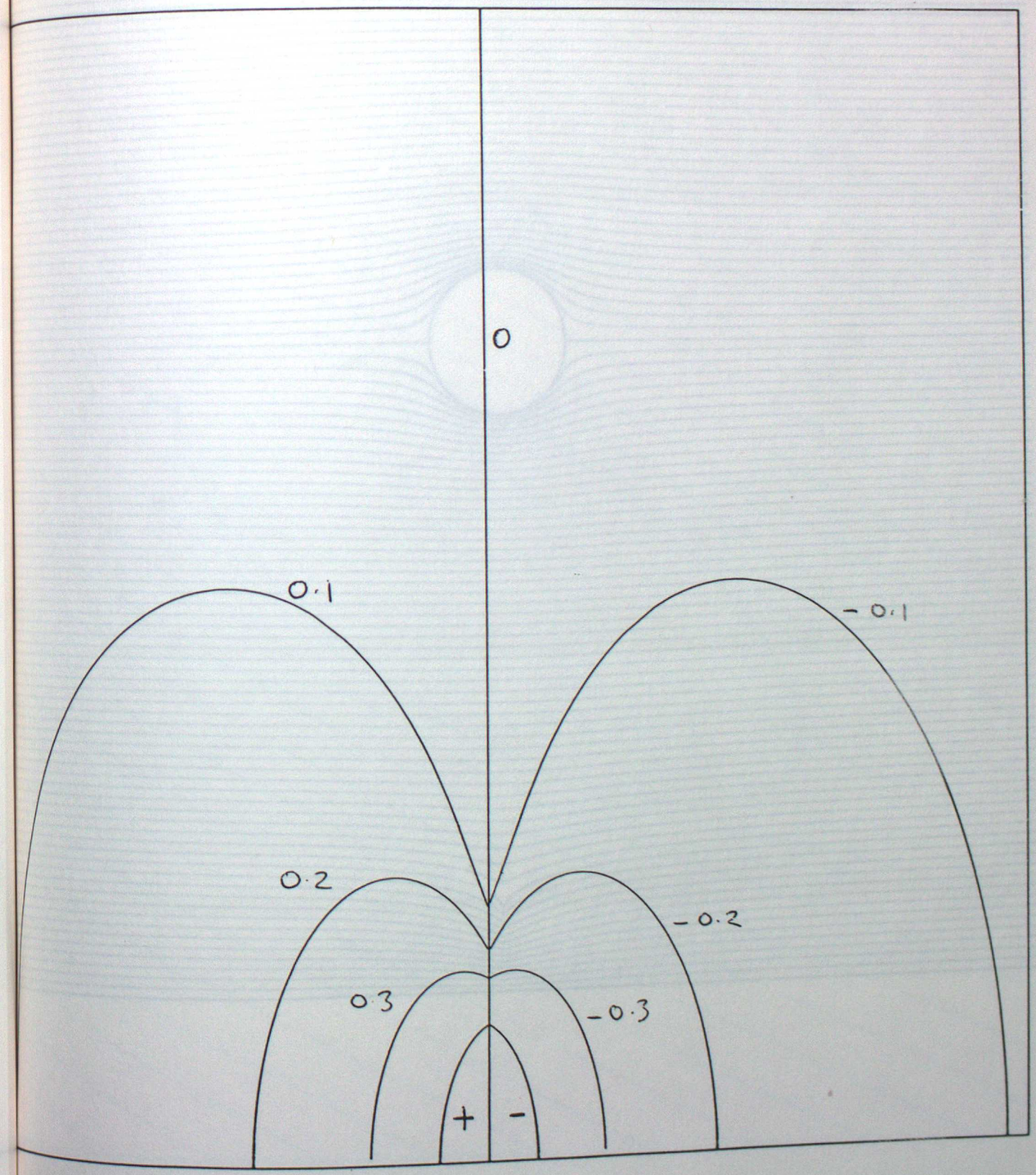

Fig. 8

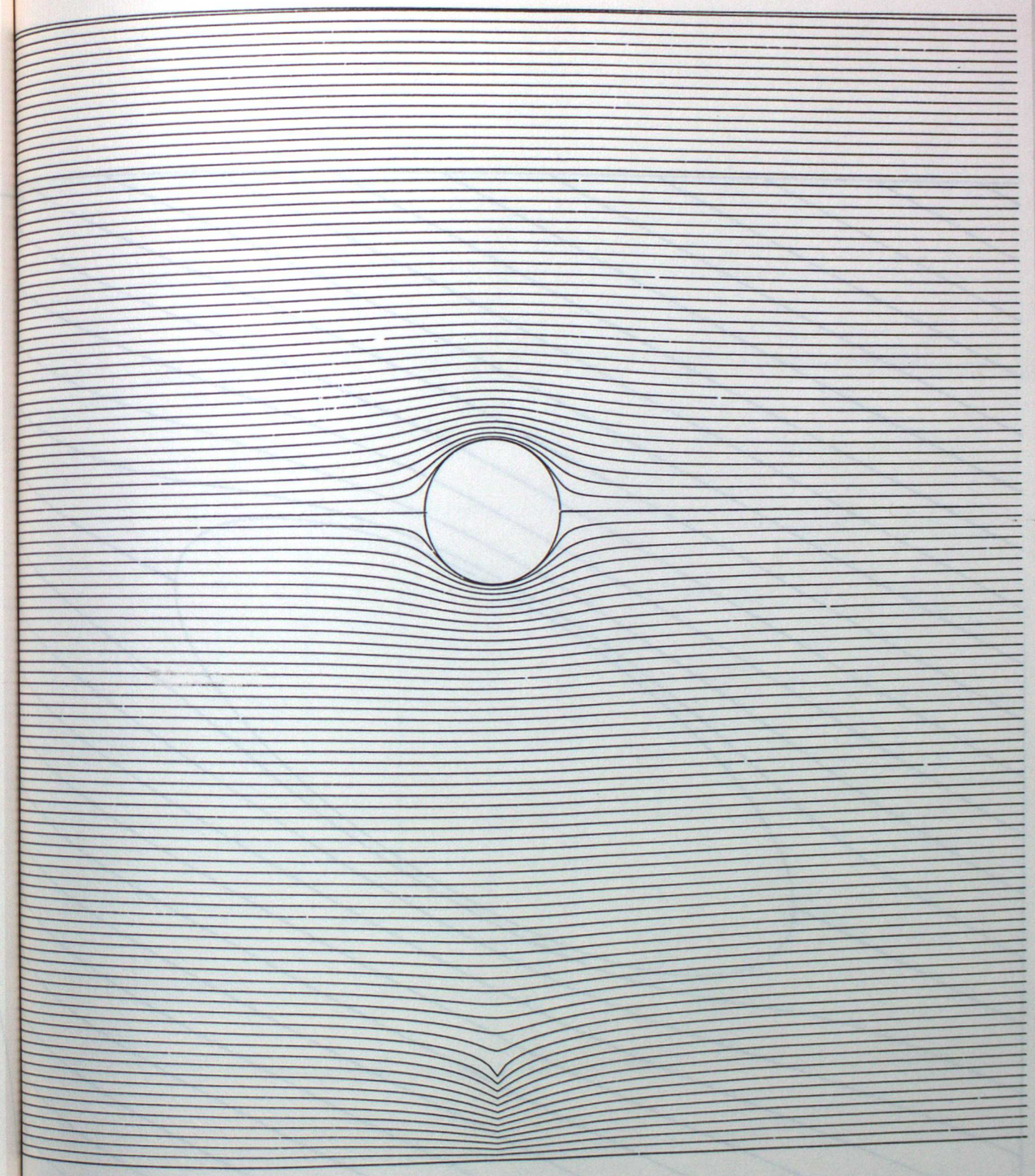

Fig. 9 (a)

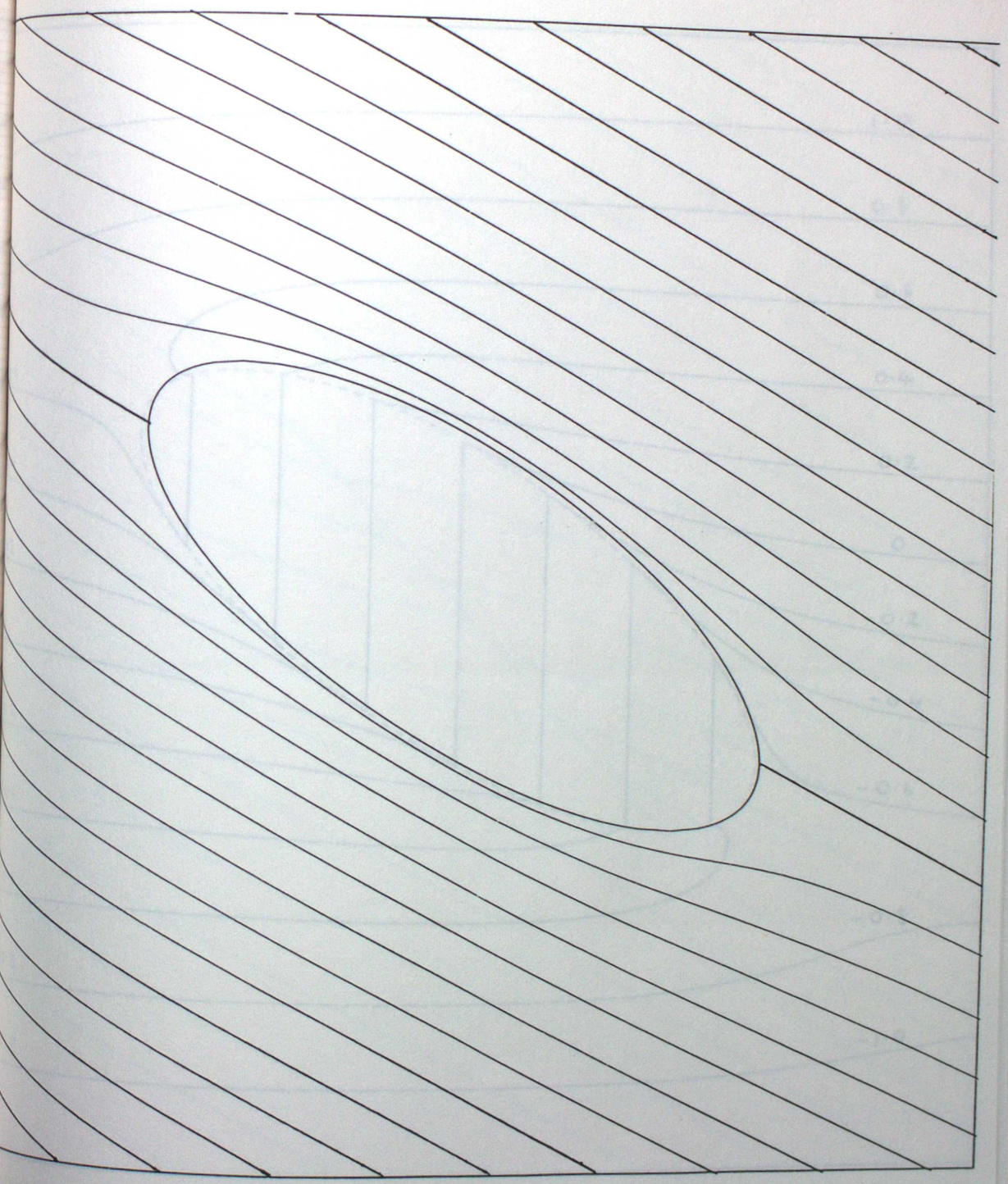

Fig. 9 (b)

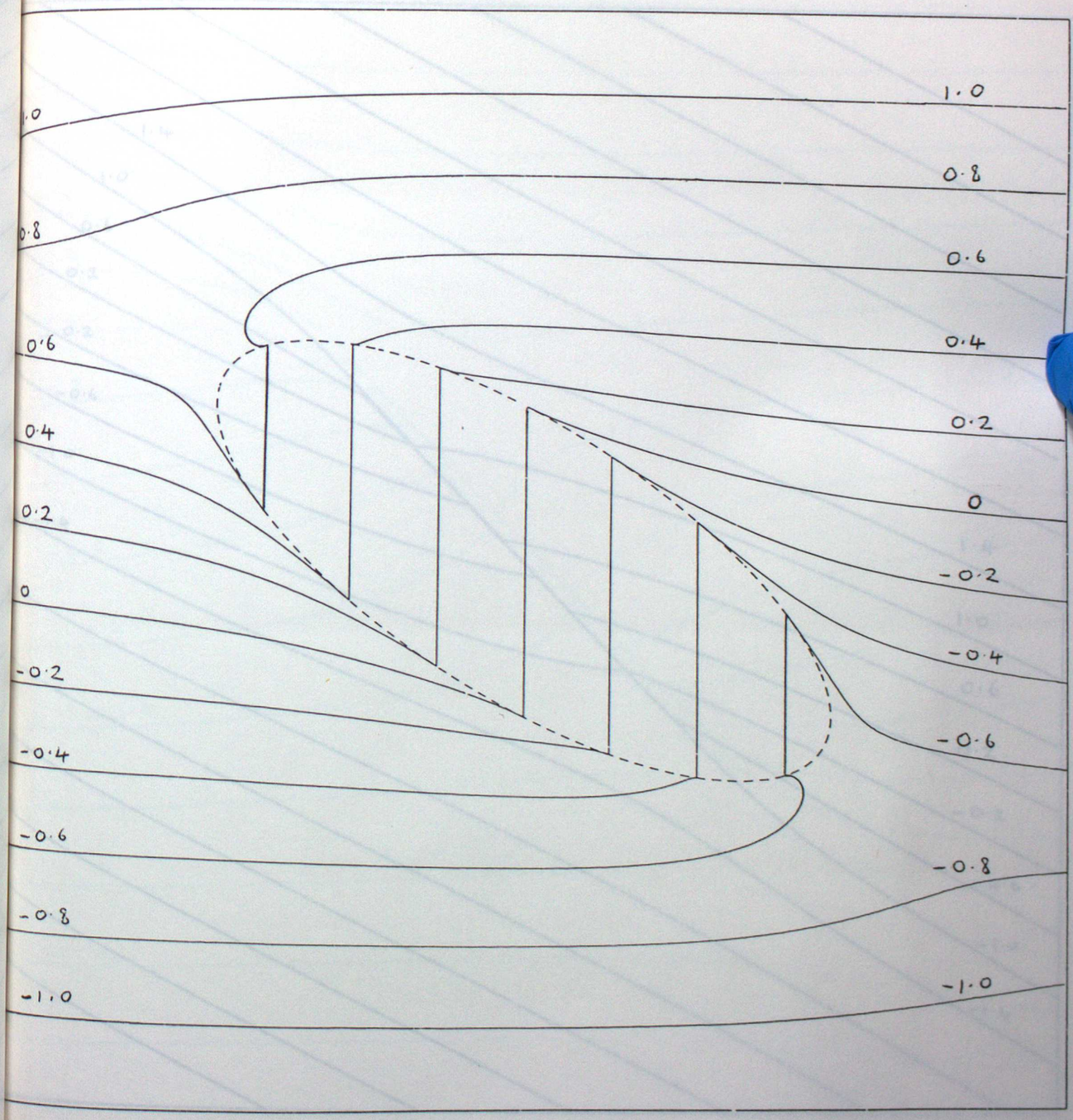

Fig. 10 (a)

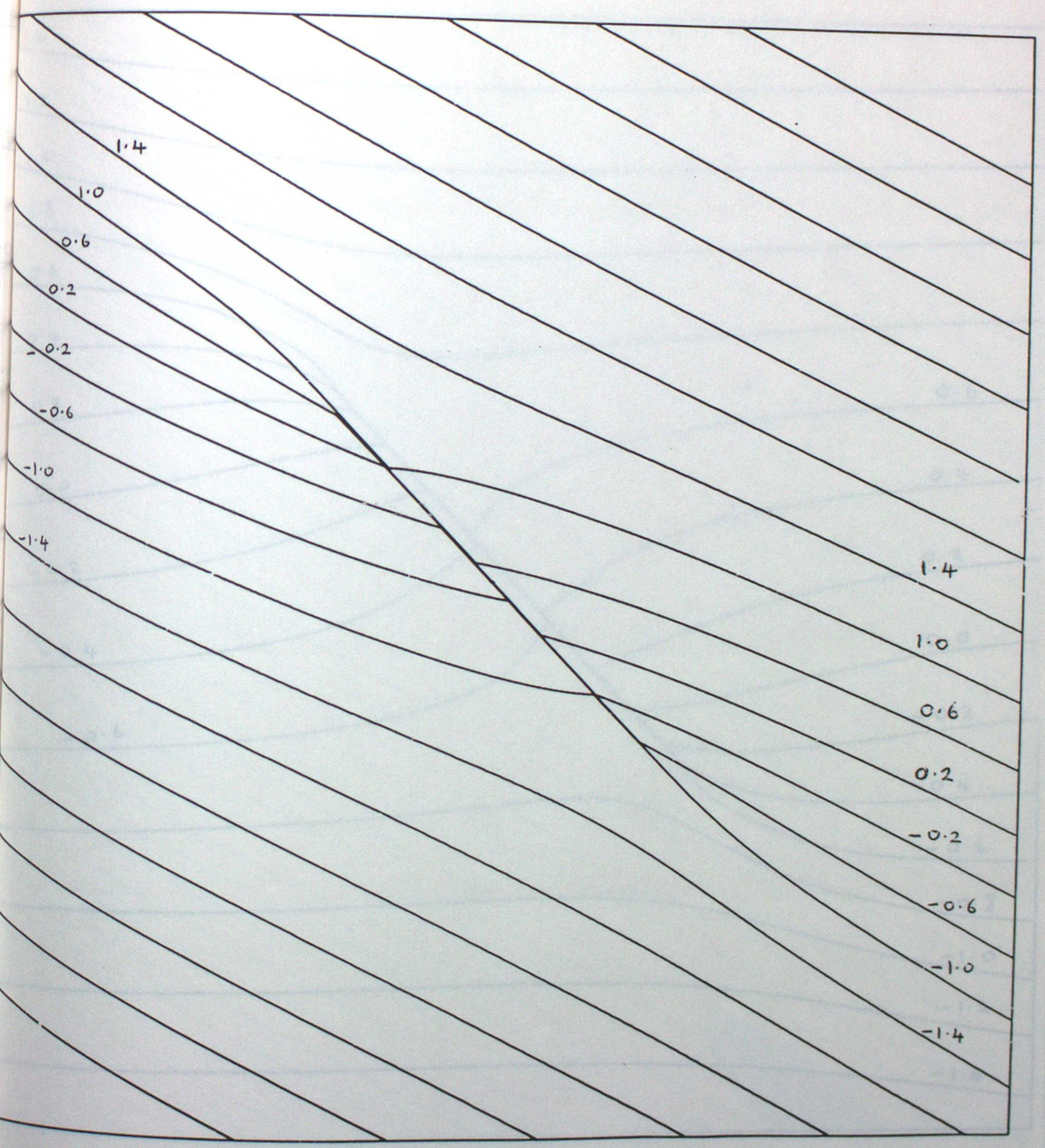

Fig. 10 (b)

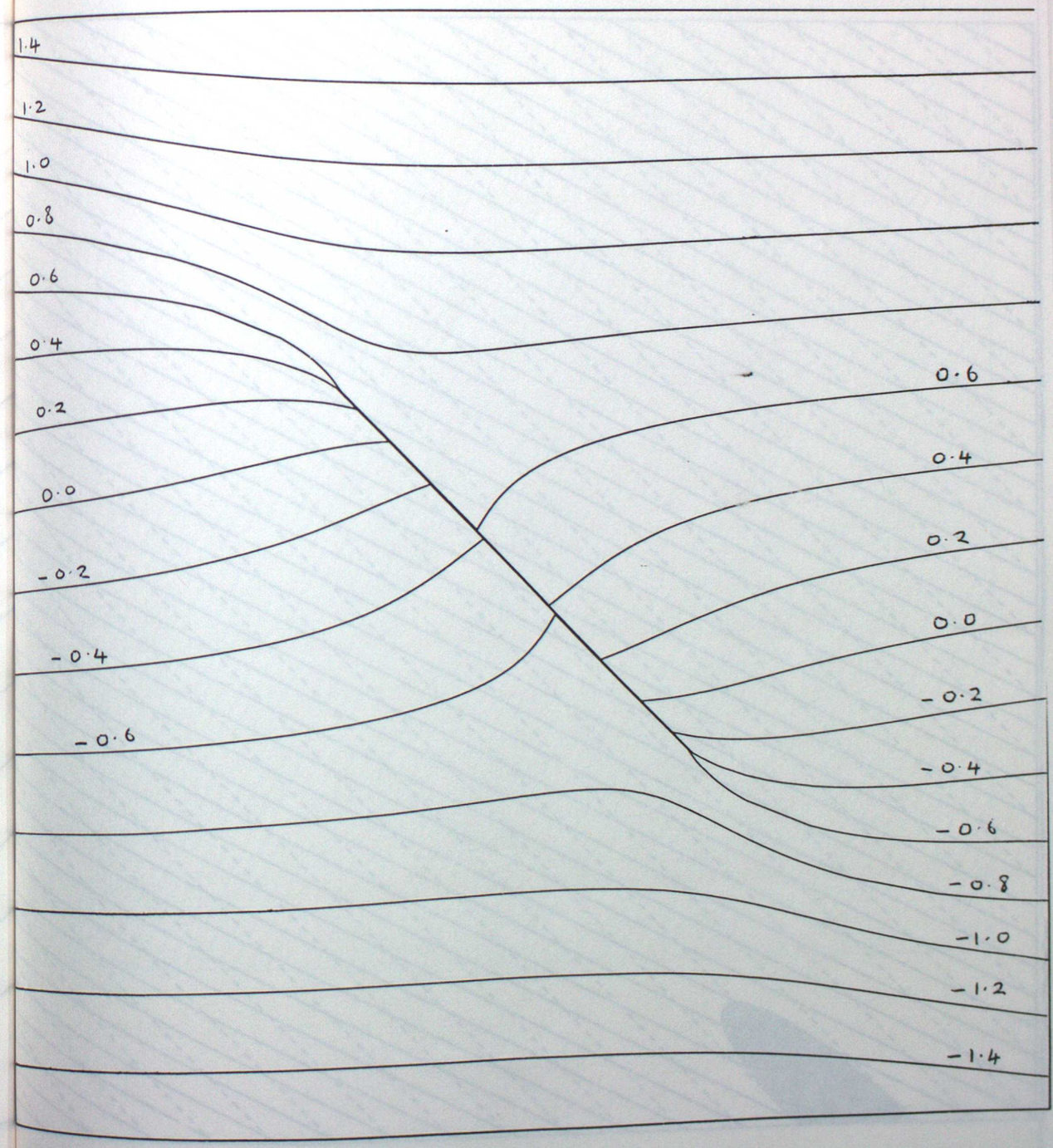

Fig. 11

Fig. 12

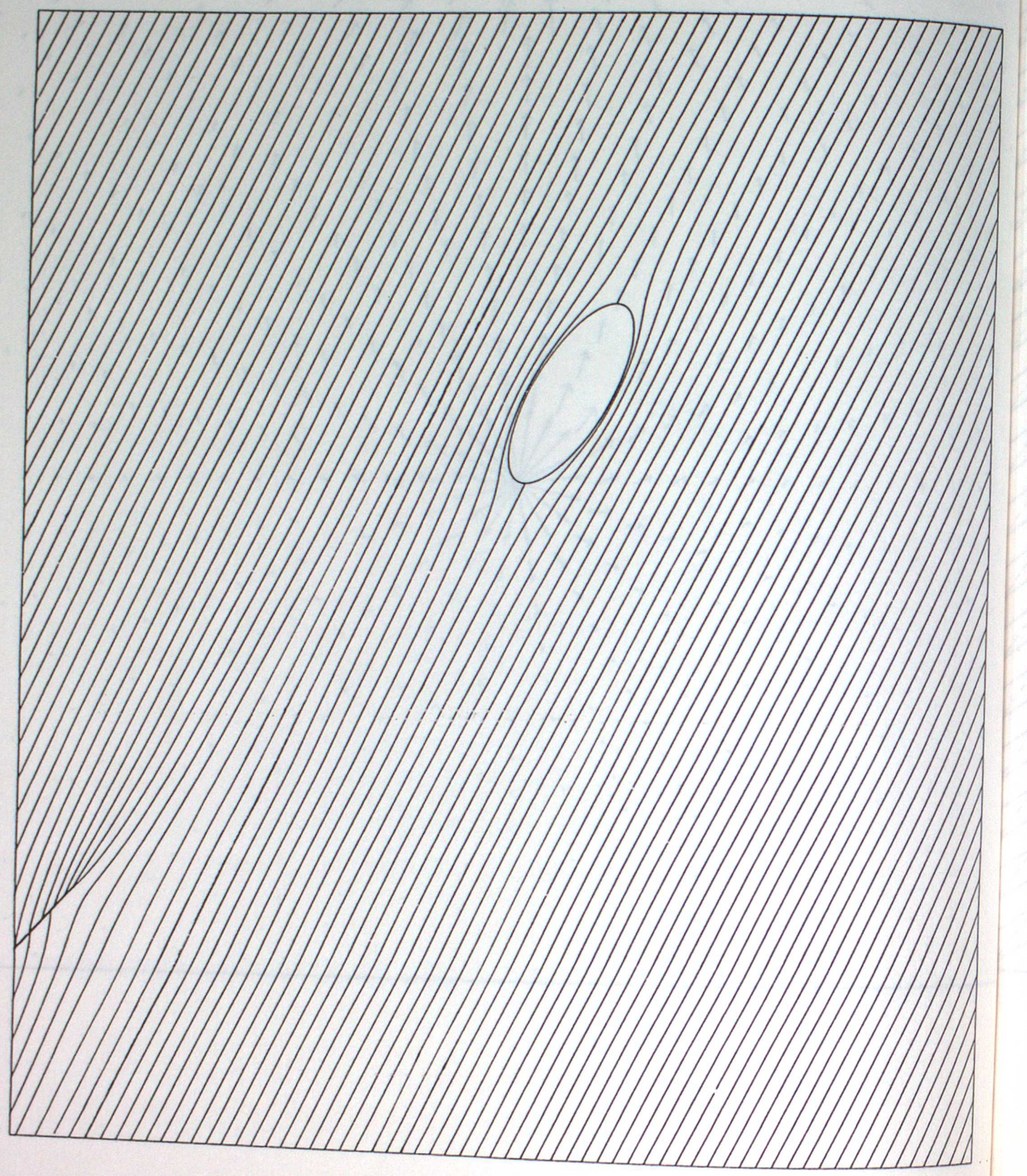

Fig. 13

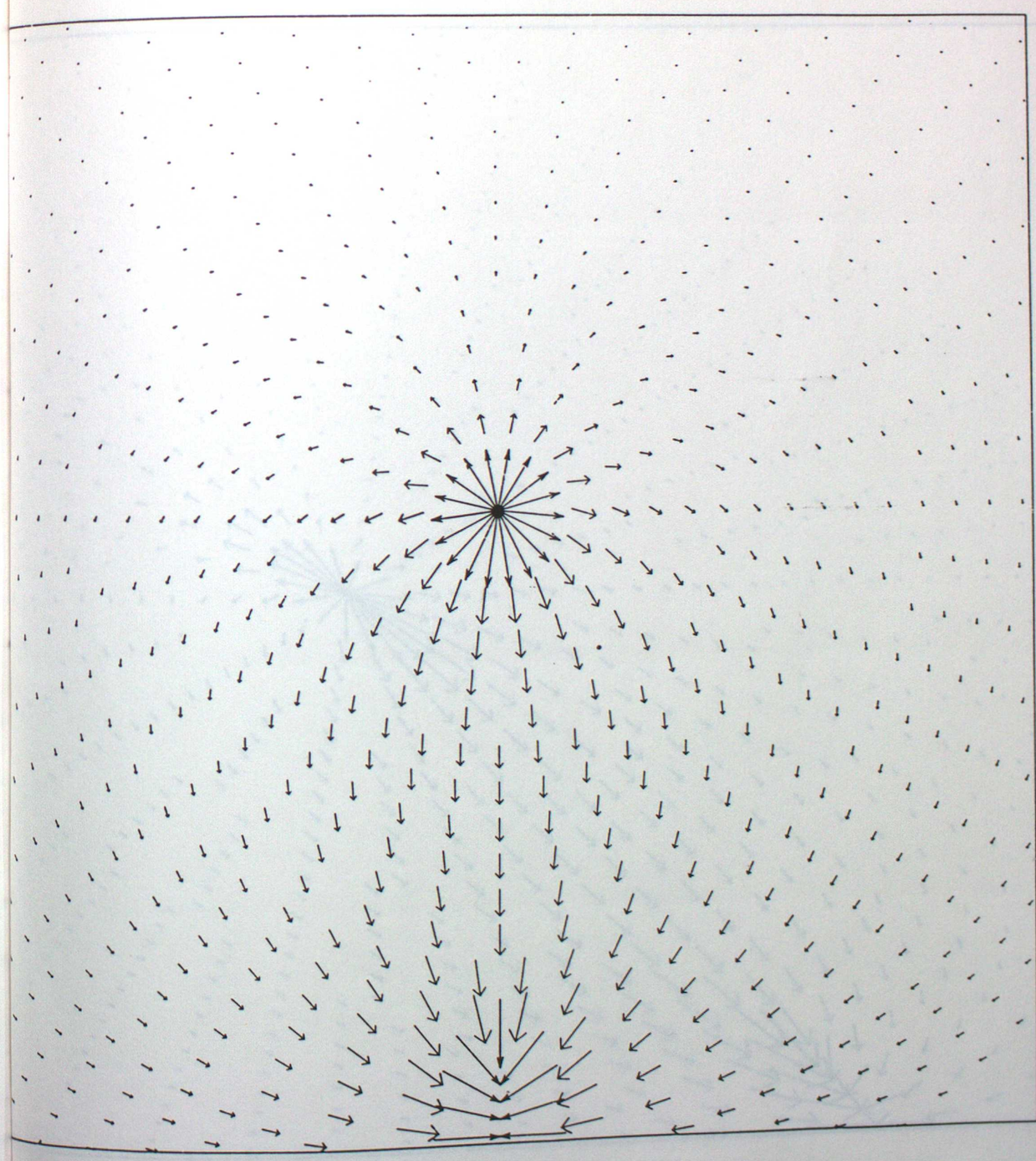

Fig. 14